THE ASTROPHYSICAL JOURNAL, 453:48–64, 1995 November 1

THE CONTRIBUTION OF LATE-TYPE/IRREGULARS TO THE FAINT GALAXY COUNTS FROM *HUBBLE SPACE TELESCOPE*[1] MEDIUM DEEP SURVEY IMAGES

SIMON P. DRIVER AND ROGIER A. WINDHORST
Department of Physics and Astronomy, Arizona State University, Tempe, AZ 85287-1504

AND

RICHARD E. GRIFFITHS
Bloomberg Center for Physics and Astronomy, The Johns Hopkins University, Baltimore, MD 21218-2695
Received 1994 October 26; accepted 1995 May 12

ABSTRACT

We present a complete morphologically classified sample of 144 faint field galaxies from the *HST* Medium Deep Survey with $20.0 \leq m_I < 22.0$ mag. We compare the global properties of the ellipticals and early- and late-type spirals and find a nonnegligible fraction (13/144) of compact blue [$(V-I) \leq 1.0$ mag] systems with $r^{1/4}$ profiles. We give the differential galaxy number counts for ellipticals and early-type spirals independently and find that the data are consistent with no-evolution predictions based on conventional flat Schechter luminosity functions (LFs) and a standard cosmology.

Conversely, late-type/irregulars show a steeply rising differential number count with slope $(\delta \log N/\delta m) = 0.64 \pm 0.1$. No-evolution models based on the Loveday et al. and Marzke et al. *local* luminosity functions underpredict the late-type/irregular counts by 1.0 and 0.5 dex, respectively, at $m_I = 21.75$ mag. Examination of the irregulars alone shows that $\sim 50\%$ appear inert and the remainder have multiple cores. If the inert galaxies represent a nonevolving late-type population, then a Loveday-like LF ($\alpha \simeq -1.0$) is ruled out for these types, and an LF with a steep faint end ($\alpha \simeq -1.5$) is suggested. If multiple core structure indicates recent star formation, then the observed excess of faint blue field galaxies is likely a result of *evolutionary* processes acting on a *steep* field LF for late-type/irregulars. The evolutionary mechanism is unclear, but 60% of the multiple-core irregulars show close companions. To reconcile a Marzke-like LF with the faint redshift surveys, this evolution must be preferentially occurring in the brightest late-type galaxies with $z \gtrsim 0.5$ at $m_I = 21.75$ mag.

Subject headings: galaxies: evolution — galaxies: fundamental parameters — galaxies: irregular — galaxies: luminosity function, mass function — galaxies: statistics — surveys

1. INTRODUCTION

The majority of explanations for the excess of faint blue galaxies (FBGs; see Broadhurst, Ellis, & Shanks 1988, hereafter BES) observed in deep ground-based CCD images (e.g., Tyson 1988; Lilly, Cowie, & Gardner 1991; Driver et al. 1994; Neuschaefer & Windhorst 1995) involve irregular/dwarf[2] populations (Kron 1980; Lacey 1991). In some models, these dwarfs have evolved rapidly through isolated starbursts (Cowie, Songalia, & Hu 1991; Babul & Rees 1992) or via general luminosity evolution (Phillipps & Driver 1995), while in other models, strong merging (Broadhurst, Ellis, & Glazebrook 1992; Rocca-Volmerange & Guiderdoni 1990) or tidally induced star formation (Lacey et al. 1993) are proposed. Other models have suggested that no evolution is necessary and that the abundance of FBGs may be the result of a combination of cosmological effects and/or an underestimation of the *local* space density of irregular/dwarf galaxies (Koo, Gronwall, & Bruzual 1993; Driver & Phillipps 1995; McGaugh 1994). Whichever process is occurring (and perhaps a combination of several), one needs high-resolution studies of a well-selected galaxy sample in the magnitude range over which the FBG excess is observed to address their true nature. Ground-based studies are always limited in resolution as a result of atmospheric seeing, because the *median* scale length of faint field galaxies is $\sim 0''.3$ (Griffiths et al. 1994b, hereafter GR94b; Casertano et al. 1995, hereafter CRGINOW). Giraud (1992) found evidence for both merging, isolated starbursts, and possibly post-starburst remnants. The studies of Burkey et al. (1994) and Colless et al. (1994) also find a significantly increased fraction of close companions for $19 \leq m_I \leq 22$ mag. The Colless et al. sample was limited by ground-based seeing to a resolution of $0''.5$–$1''.0$ FWHM. The superb resolution provided by the refurbished *HST* now allows morphological details to be seen to much higher resolution and fainter limits (Griffiths et al. 1994a, hereafter GR94a; Forbes et al. 1994; Glazebrook et al. 1995a, hereafter GL95a) and in particular allows us to study the morphology, light profiles, and contours of individual galaxies to a resolution of $\sim 0''.1$ FWHM in the flux interval over which the excess FBGs are observed (i.e., $m_B \geq 22$ mag; BES, Driver et al. 1994). Here we present a complete sample of *HST* field galaxies with *I*-band magnitudes in the range $20.0 \leq m_I < 22.0$ mag (or $22.0 < m_B < 23.5$), from which we extract a complete subsample of galaxies which are irregular in appearance. In § 2 we summarize the new *HST* WFPC2 data and its method of data reduction. In § 3 we present the detection and photometry algorithms used to construct the current catalog. In § 4 we discuss the morphological classification, and in § 5 we compare the global properties of

[1] Based on observations with the NASA/ESA *Hubble Space Telescope* obtained at the Space Telescope Science Institute, which is operated by AURA, Inc., under NASA contract NAS 5-26555.

[2] Here we broadly define dwarf galaxies to have $M_B \geq -18.0$ mag for $H_0 = 50\,\mathrm{km\,s^{-1}\,Mpc^{-1}}$, i.e., galaxies like the LMC and fainter.

each galaxy class. In § 6 we present a discussion of the detailed morphology of the irregular *HST* galaxies.

2. THE *HST* WFPC2 DATA

The *HST* Medium Deep Survey (MDS) collects data in parallel with other *HST* instruments (FOC, FOS, FGS) using the WFPC2 to randomly image a field 4′–14′ away from the primary target (depending on the primary *HST* instrument being used). A more detailed description of the MDS project is given by GR94b, and a summary of the Cycle 4 *HST* data reduction methods is given by Ratnatunga et al. (1995). The MDS pipeline data reduction was carried out using the MDS WFPC2 super-skyflats (Ratnatunga, Griffiths, & Casertano 1994). This results in a uniform calibration accuracy of ± 0.1 mag (Holtzman et al. 1995). The actual zero magnitude points for 1.0 ADU s^{-1} are $K_{I_{814W}} = 21.67 - 0.009$(F606W − F814W) mag and $K_{V_{606W}} = 22.84 - 0.076$(F555W − F814W) mag. [Note that (F606W − F814W) $\simeq 1.4$ and (F555W − F814W) $\simeq 1.8$ mag for faint field galaxies; GR94a, GR94b]. The fields were selected from the MDS database to have comparable exposure times in both the wide V (F606W) and I (F814W) filters. Table 1A shows the positions and exposure times for the data used in this study, along with Galactic foreground extinction in V_{606} and I_{814}, taken from the reddening values in Burstein & Heiles (1982). We adopted an extinction $\propto 1/\lambda$ (Osterbrock 1989) and a ratio of $A_V/E(B-V) = 3.2$. The removal of cosmic rays was achieved using the CRREJECT facility in IRAF's IMCOMBINE, which compares individual orbits to reject cosmic rays and creates a final stack via a sigma-weighted average. In general, we did not have a sufficient number of undithered orbits per field to apply the optimized CR rejection routines of Windhorst, Franklin, & Neuschaefer (1994). Additional low-level cosmic rays and bad pixels were therefore cleaned by replacing pixel values 3 σ above or below the local median sky background with the mean from adjacent pixels. The WFC pixel scale is 0.″0996 pixel^{-1}, and so each of the three WFC CCDs corresponds to a 1.′3 × 1.′3 region.[3] This gives a total sky coverage of 0.00845 deg^2. Data from the PC were not used in this survey owing to their poorer surface brightness (SB) sensitivity and their much lower sky coverage.

3. A COMPLETE CATALOG OF IRREGULAR *HST* GALAXIES TO $m_I = 22$ mag

In order to define a complete sample of irregular *HST* galaxies and study their morphology in an unbiased way, it was necessary first to construct a complete sample for *all* galaxy types from the MDS images. Therefore we required that the magnitude limit was not so faint that the irregulars become unresolvable by *HST*. Typical field irregulars are expected in the range $20.0 \lesssim m_I \lesssim 22.0$ mag and $0.''5 \lesssim r_{\text{half-light}} \lesssim 1''$ for $z \lesssim 0.3$, assuming $-14.5 \lesssim M_I \lesssim -19.5$ mag, $(B-I) \simeq 1.5$, and $r_{hl} \simeq 1$–3 kpc (for $H_0 = 50$ km s^{-1} Mpc^{-1}, $q_0 = 0.5$, and $\Lambda = 0$). This observed range is equivalent to a B-band magnitude range of $22.0 < m_B < 23.5$ (Driver et al. 1994), at which level the observed density of FBGs is a factor of ~ 2–3 over the standard cosmological predictions (Tyson 1988; see our figures in § 5). The expected surface density of galaxies of *all* types in this I-band range is ~ 20 objects per WFPC2 field (Tyson 1988; Driver et al. 1994; Table 1B here).

[3] There is a potential bias introduced by the position of the primary *HST* target and the desire for long integrations. However, most primary targets are themselves randomly detected (i.e., QSOs or stars at relatively high galactic latitude), so any such bias is expected to be small.

TABLE 1A

FIELD POSITIONS AND EXPOSURE TIMES FOR SELECTED MDS FIELDS

FIELD NAME	R.A. (J2000)	decl. (J2000)	l^{II}	b^{II}	EXPOSURE TIME V	EXPOSURE TIME I	NUMBER OF ORBITS V	NUMBER OF ORBITS I	$A_{V_{606}}$ (mag)	$A_{I_{814}}$ (mag)
ueh0	00:53:23.2	+12:33:58	123°68	−50°30	8700	6300	5	3	0.13	0.10
uim0	03:55:31.6	+09:43:34	179.83	−32.15	8800	5200	12	6	0.31	0.23
uop0	07:50:47.1	+14:40:44	206.07	19.63	7200	4200	5	2	0.04	0.03
usa2	17:12:23.2	+33:35:49	56.72	34.25	5400	6300	3	3	0.08	0.06
ux40	15:19:41.2	+23:52:06	35.78	56.51	3300	7500	2	4	0.10	0.07
uy40	14:34:48.7	+25:08:02	33.87	66.75	5200	6000	6	6	0.06	0.04

TABLE 1B

STATISTICS AND DETECTIONS FOR THE SELECTED MDS FIELDS

FIELD	K_V	K_I	$2\sigma\mu_V$	$2\sigma\mu_I$	NUMBER OF DETECTIONS[a] WFC2	WFC3	WFC4
ueh0i	33.23	32.45	23.8	23.4	7	11	7
uim0i	32.53	31.48	24.2	23.4	8	6	5
uop0i	33.09	32.45	24.3	23.3	5	10	12
usa2i	33.33	32.45	25.0	24.3	6	7	14
ux40i	33.23	32.32	23.5	24.1	9	6	9
uy40i	32.53	31.64	24.7	23.9	7	12	3

NOTE.—K_V and K_I are the calibration constants for the V and I fields, respectively, with the exposure time and a scaling factor incorporated (i.e., observed mag = $K - 2.5$ log ADU$_{tot}$).

[a] Total number of detections = 144.

3.1. *Image Detection and Photometry*

Prior to the image detection phase, a median filter of 127 × 127 pixels was used to create a smoothed sky image for each WFPC2 frame, representing any large-scale variations in the sky (gradients of ~2% typically remained after applying the MDS supersky flats). This sky image was subtracted from the original frame to give an extremely flat sky background (≪2%). We divided each CCD frame into nine sections and measured the sky background within each section, using a Gaussian fit to the peak of the analog-to-digital convertor unit (ADU) histogram, which reduced the WFPC2 gradients of 2%–3% to ≲0.5% of sky.

The initial object detection was done with the isophotal detection routine IMAGES in the RGASP package (Cawson 1983), searching for objects with four connected pixels (0.04 arcsec^2) with a signal 2 σ above the mean sky background (where σ is the measured noise in the *local* sky background). Detections with centroids within 26 pixels (2.″6) of the CCD frame edge were rejected to prevent any edge bias. This reduces the usable area per CCD image to 660^2 pixels or 1.′1 × 1.′1. For the photometry stage, we used a variable size circular aperture centered on the initial detection position and a global sky background for each CCD image (because any significant large-scale structure in the sky background was already removed to ≲0.5% or ~28.5 mag arcsec^{-2}). The size of the aperture, r_{ap}, was based on the following relationship:

$$r_{ap}^n = r_{iso}^n + r_{min}^n , \quad (1)$$

as described in Driver (1994) and in Jones et al. (1995). This equation essentially satisfies the condition that the aperture radius is comparable to the isophotal radius r_{iso} for objects with large isophotal areas (i.e., bright), and comparable to a *fixed* minimum r_{min} for objects with small isophotal radii (i.e., faint). The following optimal values for pure exponential disks were determined via simulations (Driver 1994): $n = 1.5$ and $r_{min} \simeq 1'' \simeq 3$ scale lengths (CRGINOW). These simulations showed that this technique includes at least 95% of the light for exponential disks as well as bulge-dominated galaxies. All detections with an aperture flux $m_I \leq 22.0$ mag were reevaluated individually to exclude any contamination resulting from nearby objects within the initial aperture. The final catalog was then defined to be all galaxies within the *total* flux range of $20.0 \leq m_I < 22.0$ mag.

3.2. *Completeness of the HST WFPC2 Sample*

Figure 1 shows the logarithm of the signal-to-noise ratio versus *I*-band magnitude for the isophotal detection stage (Fig. 1*a*) and the photometry stage (Fig. 1*b*) as a test of our sample completeness. The majority of detected galaxies are well above the signal-to-noise limit set by the detection criterion (i.e., 2 σ above sky over four contiguous pixels). Figure 1*b* also follows the predicted slope of −0.6 in a Euclidean universe (shown as dashed line) very closely for optimal aperture radii (i.e., the radius which just encompasses the object). Galaxies with central SB $\mu_I \geq 23.26$ mag arcsec^{-2} (i.e., whose extent is greater than 5″ in radius; see Table 1B) would escape detection. Since no objects are seen close to the quoted signal-to-noise limit (≃4.0 in Fig. 1*a*), the sample is essentially 100% complete down to a limiting *total* magnitude of $m_I = 22.0$ mag. A discussion of the completeness of WFC images much closer to the *HST* detection limit is given by Neuschaefer et al. (1995). Note that the total *volume* surveyed for low-SB galaxies is still very small as a result of the limited WFC2 field-of-view. The catalog may therefore be statistically misrepresented for these types (Disney 1976). Table 1B shows the number of detections per WFPC2 CCD along with the magnitude zero points and SB detection limits. The number of detections agrees well with that expected (§ 5.1).

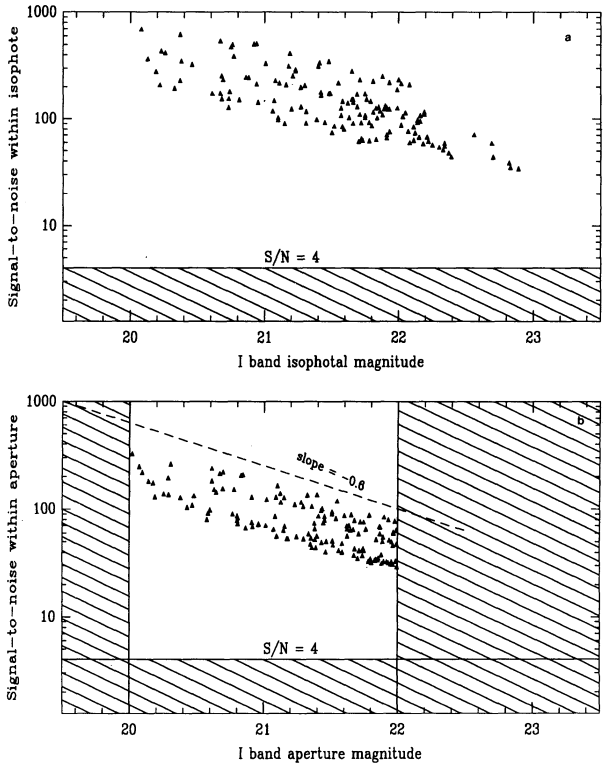

FIG. 1.—(*a*) Signal-to-noise ratio vs. magnitude for the *isophotal* detection stage. (*b*) Same as Fig. (1*a*), but for the *aperture* photometry stage. The horizontal line represents the minimum detectable signal-to-noise ratio from the detection criterion, and the vertical lines represent the selected magnitude range. Only those galaxies included in the final sample are shown here. The dashed line is the noncosmological relation between signal-to-noise ratio vs. aperture magnitude expected for a single nonevolving galaxy.

3.3. *Morphological Classification of the WFPC2 Galaxies*

The morphological classification of the *HST* galaxies was achieved from the consensus of three independent eyeball classifiers (S. P. D., R. A. W., and Roger Rouse [R. R.]). To assist in the classification, gray-scale plots were made from 1 σ below sky to 5 σ above sky, as well as major-axis profiles in both SB versus r and SB versus $r^{1/4}$. These were used to classify all objects in *both* V and I. Simulated light profiles of perfect de Vaucouleurs laws and exponential disks were also plotted on the same scales as a reference. The following rules were followed for the classification of our *HST* galaxies, based on the Hubble Atlas of Galaxies (Sandage 1961):

1. Visually compact objects showing a predominantly linear profile in SB versus $r^{1/4}$ were classified as *E*/*S*0. This includes compact systems which show no evidence for a disk, *irrespective* of their colors.

2. Objects which are linear in $r^{1/4}$ in the inner region and linear in r in the outer region were classified as "Sa," "Sb," or "Sc," depending on the ratio between the linear sections and the steepness of the respective profiles (see, e.g., Windhorst et

al. 1994a, b). Note that the Sa's, Sb's, and Sc's are lumped together into a single galaxy class for the purpose of classification in this paper. This class thus includes those systems that have a well-defined bulge and disk.

3. Objects with a flat light profile, a profile which rises from the center, an erratic profile, or a profile which is a poor linear fit to either SB versus r or SB versus $r^{1/4}$ were classified as "Sd/irregular" or "peculiar." Peculiar galaxies are those which exhibited a strong central core (initially linear in SB versus $r^{1/4}$), but with a highly disturbed outer disk. This is an attempt to distinguish between genuine irregulars and early-type galaxies undergoing some form of interaction, etc.

Note that major-axis light profiles were used rather than azimuthally averaged profiles to prevent any irregular structure being smoothed out. In all cases, the gray-scale plots were used as a secondary check to determine whether a nearby companion might be disturbing the light profiles. Both the V and I light profiles *and* gray-scale plots were used for optimal classification. Figure 2 shows a selection of major axis profiles to illustrate the range of Hubble types and light profiles seen in our *HST* sample. A representative galaxy for each Hubble class was chosen with $m_I \sim 21.5$ mag to allow a direct comparison of the appearance and light profiles of the fainter objects.

Comparing the results between the three independent classifiers, we find complete agreement for 91/144 objects and agreement to one Hubble class for 45/144 objects. The remaining eight objects were typically unusual cases where one classifier identified the major component of a clump and the other classified the entire system as "peculiar" or irregular. In these cases, the classification of the objects was openly discussed, and a consensus classification was assigned. No attempt was made to separate stars from compact ellipticals, since the two populations sometimes appear indistinguishable by visual examination of their *HST* light profiles (see Ratnatunga et al. 1995 for an automated method of star-galaxy separation). Currently, a full spectroscopic follow-up of the entire sample is in progress (Driver et al. 1995b) to determine redshifts and luminosities. This will allow an accurate separation between compact ellipticals and stars, and enable us to confirm the eyeball classifications and determine how many high-SB galaxies are masquerading as stars at faint magnitudes (CRGINOW).

3.4. *Reliability of the WFPC2 Classifications*

Figure 3 shows a simple test of our classification by plotting the concentration index (C.I. = core SB minus total magnitude) versus total magnitude. Here the core SB is defined as the flux within 0".2 radius in units of magnitudes per square arcsecond. The C.I. is a measure of the concentration of galaxy light, where a lower index reflects a greater amount of light contained in the core, which is expected to correlate well with morphological type (Forbes et al. 1994). This should not be confused with the more conventional definition of the C.I. (e.g., Kent 1985), which requires better resolution and signal-to-noise ratio than we have. In reality, the core SB is both resolution and distance dependent. However, at moderate redshifts, the Θ-z relation for *HST* bulges and disks is flat enough (Mutz et al. 1994) that the C.I. is distance independent to first order.

Figure 3 shows that the E/S0 sample (i.e., compact systems including a small number of stellar-like objects) separates very well from the bright spirals. However, the transition from early- to late-type spirals is less well defined by this technique, although there is still a distinct correlation between galaxy type and the C.I.

As a final check, we compare our morphological classifications to those of GL95a and GR94a. Both these surveys are also based on *HST* MDS data. The survey of GL95a covers several fields in common with this study yet uses entirely independent methods for data reduction and image detection. Comparing the classifications for the 92 galaxies in common, we find that 25 agree exactly, 44 within one Hubble class, and 8 within two Hubble classes. The remaining 14 objects are unusual in some way and represent cases in which a decision had to be made as to whether to classify the major component of a clump or the entire system. In their magnitude-limited sample, GR94a find a mixture of 19% E/S0, 44% Sa-Sm, 13% irregulars/mergers, and 25% peculiar/unclassified, whereas we find 32% E/S0, 53% Sa-Sd, and 15% irregular/peculiar. The agreement clearly depends on the distribution of the peculiar/unclassified class of GR94a among our classes, but they note that a significant number (i.e., about half) of their "unclassified objects" were classified as S0's by one of their two classifiers. If so, this would suggest very good agreement between the two samples. Overall, we consider the agreement between this study and those of GL95a and GR94a to be good, providing a consistent picture of the field galaxy mix at faint magnitudes.

Nevertheless, we recognize the need to develop an automated classifier for faint field galaxies. Given the good agreement with the other independent eyeball classifiers of GL95a, we consider our sample to be a suitable representative control set and thus a good training set for neural network classifiers. Such automated classification methods are essential, since the MDS database of WFPC2 images has by now accumulated over 200 fields containing several thousand galaxies. Finally, we note that a full spectroscopic survey is underway, which will help confirm the reliability of these classifications, although we point out that faint E/S0's and Sa's, as well as faint Sb's and Sc's, are hard to distinguish spectroscopically at moderate redshifts (Keel & Windhorst 1993; Windhorst et al. 1994a, b).

3.5. *The WFPC2 Galaxy Catalog down to $I \leq 22$ mag*

Table 2 shows the full WFPC2 catalog which contains the basic parameters for the 144 MDS field galaxies from which we draw our irregular galaxy sample. The random error in the listed magnitudes is ± 0.06 mag. The largest error comes from the limited accuracy in the sky subtraction. Given that large-scale residuals in the sky are of order 0.5%, an average aperture radius of 16 pixels (see col. [14] of Table 2) yields random errors of $\sigma_I = 0.06$ and $\sigma_V = 0.10$ mag for an object with $I = 22.0$ and $V = 23.3$ mag (and a mean sky value of $\mu_I = 21.7$ and $\mu_V = 22.3$ mag arcsec^{-2}). For the $(V-I)$ color, this implies a random error of ± 0.12 mag.

More information about the objects in Table 2, such as their scale lengths, is given by Ratnatunga et al. (1995). A discussion of the scale lengths of MDS galaxies is also given by Mutz et al. (1994) as a function of redshift, and by CRGINOW and Im et al. (1995a) as a function of apparent magnitude.

The classifications in Table 2 are listed according to Hubble class as defined above. For the remainder of this paper, the Hubble classifications that we assigned to the individual WFPC2 galaxies were binned into three classes: E/S0 (compact), Sabc (early-disk), and Sd/irregular (late-disk) plus peculiar galaxies. The Sd's were grouped together with irregulars to obtain roughly equal numbers in each of the three categories.

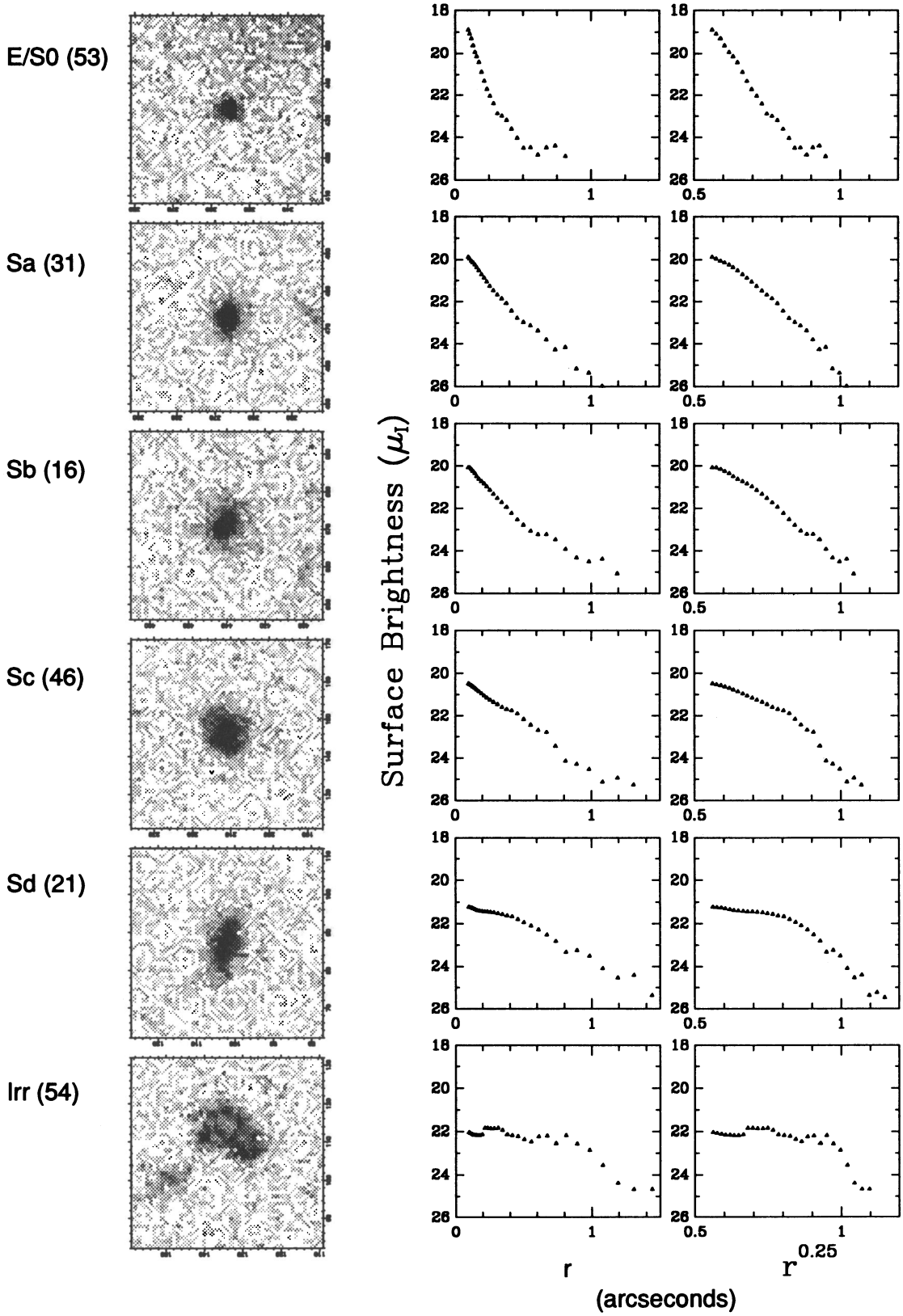

FIG. 2.—A selection of gray-scale plots and major-axis light profiles used for the eyeball classifications. The gray-scale plots are plotted as log (intensity) from $\mu_I = 21.0$ mag arcsec^{-2} to sky. Major axis profiles are shown as SB vs. radius (r) and SB vs. $r^{1/4}$. A representative galaxy for each morphological class is shown at comparable magnitudes ($m_I \sim 21.5$ mag). Only the I-band data are shown here, but equivalent V-band data were also used in the classification process.

TABLE 2

A COMPLETE CATALOG OF *HST* FIELD GALAXIES OBTAINED FROM THE SIX MDS FIELDS

ID (1)	Field (2)	Chip (3)	X (4)	Y (5)	RA(J2000) (6)	DEC(J2000) (7)	I (8)	V-I (9)	Ic (10)	(V-I)c (11)	e (12)	T (13)	ApRad (14)
1	ueh0i	2	572.4	724.9	00:53:25.89	+12:32:41.2	20.42	1.47	19.44	1.51	0.15	1	17
2	ueh0i	2	87.5	266.8	00:53:23.65	+12:33:38.5	20.81	0.93	19.73	1.05	0.47	1	15
3	ueh0i	2	137.2	142.3	00:53:24.21	+12:33:48.9	20.87	1.35	20.80	1.47	0.63	4	18
4	ueh0i	2	644.1	394.5	00:53:27.01	+12:33:10.4	21.07	0.61	20.44	0.79	0.09	2	15
5	ueh0i	2	758.2	493.6	00:53:27.55	+12:32:57.8	21.38	1.35	20.14	1.45	0.19	2	14
6	ueh0i	2	771.1	79.3	00:53:28.43	+12:33:36.7	21.35	0.88	21.96	0.96	0.52	5	16
7	ueh0i	2	146.1	364.0	00:53:23.83	+12:33:27.6	21.68	0.20	19.23	0.12	0.13	0	13
8	ueh0i	3	520.0	255.0	00:53:21.56	+12:33:22.3	20.80	1.17	20.38	1.20	0.20	3	16
9	ueh0i	3	674.9	196.0	00:53:21.63	+12:33:05.9	20.91	1.59	19.53	1.59	0.34	1	15
10	ueh0i	3	385.3	99.5	00:53:22.83	+12:33:30.6	20.96	1.39	19.64	1.40	0.31	1	15
11	ueh0i	3	444.8	746.8	00:53:18.52	+12:33:43.7	21.16	1.66	18.84	1.38	0.11	0	13
12	ueh0i	3	172.6	158.8	00:53:22.87	+12:33:52.4	21.15	0.69	19.76	0.43	0.39	2	15
13	ueh0i	3	221.6	81.7	00:53:23.27	+12:33:45.6	21.34	2.01	19.01	1.98	0.06	0	13
14	ueh0i	3	726.2	349.5	00:53:20.53	+12:33:05.6	21.30	1.14	20.96	1.27	0.77	4	15
15	ueh0i	3	290.2	412.6	00:53:20.99	+12:33:48.8	21.36	1.13	20.07	1.05	0.09	1	14
16	ueh0i	3	721.4	490.4	00:53:19.64	+12:33:10.1	21.52	1.64	20.06	1.78	0.37	2	14
17	ueh0i	3	612.9	426.9	00:53:20.26	+12:33:18.5	21.68	1.19	21.58	1.58	0.84	4	15
18	ueh0i	3	127.1	721.3	00:53:19.33	+12:34:13.0	21.90	1.28	22.20	0.99	0.53	5	14
19	ueh0i	4	238.7	418.9	00:53:23.38	+12:34:43.5	20.81	1.23	20.52	1.27	0.06	3	17
20	ueh0i	4	665.1	135.1	00:53:20.05	+12:34:29.5	21.35	1.32	21.55	1.35	0.47	4	16
21	ueh0i	4	136.8	152.4	00:53:23.49	+12:34:15.2	21.56	1.01	21.22	1.04	0.62	4	15
22	ueh0i	4	477.8	181.6	00:53:21.35	+12:34:28.2	21.86	1.03	20.37	1.26	0.37	1	14
23	ueh0i	4	229.7	299.3	00:53:23.19	+12:34:31.8	21.84	0.67	21.17	0.73	0.89	4	14
24	ueh0i	4	464.1	561.6	00:53:22.22	+12:35:03.8	21.85	0.90	20.42	0.71	0.34	1	14
25	ueh0i	4	475.9	639.6	00:53:22.30	+12:35:11.5	21.96	0.92	21.70	0.90	0.23	4	14
26	uim0i	2	289.9	439.3	03:55:31.76	+09:42:47.5	20.19	1.16	19.50	1.21	0.77	1	17
27	uim0i	2	374.6	156.8	03:55:33.41	+09:43:03.7	20.25	1.19	18.83	0.00	0.25	1	15
28	uim0i	2	773.5	743.8	03:55:32.95	+09:41:53.9	21.40	0.75	18.89	0.73	0.10	0	13
29	uim0i	2	457.6	704.1	03:55:31.49	+09:42:16.7	21.96	0.58	23.43	-0.15	0.89	6	15
30	uim0i	2	304.7	282.5	03:55:32.51	+09:42:58.5	21.51	2.03	19.18	1.69	0.05	0	13
31	uim0i	2	523.0	416.7	03:55:33.06	+09:42:34.4	21.59	1.62	19.88	1.77	0.73	1	13
32	uim0i	2	248.5	540.5	03:55:31.11	+09:42:42.3	21.75	1.86	20.26	1.93	0.02	1	13
33	uim0i	2	350.8	612.1	03:55:31.33	+09:42:30.4	21.95	1.41	21.96	1.31	0.84	5	15
34	uim0i	3	626.8	153.7	03:55:29.18	+09:42:56.0	20.14	1.37	17.82	1.31	0.14	0	13
35	uim0i	3	110.6	575.8	03:55:29.23	+09:44:02.0	20.60	1.48	19.43	1.38	0.31	1	16
36	uim0i	3	367.4	366.8	03:55:29.21	+09:43:29.3	21.25	1.33	21.67	1.55	0.08	4	16
37	uim0i	3	242.2	615.5	03:55:28.46	+09:43:54.6	21.74	1.18	20.23	1.03	0.30	1	13
38	uim0i	3	373.6	555.7	03:55:28.20	+09:43:40.8	21.71	1.13	21.90	1.08	0.45	5	14
39	uim0i	3	368.9	606.8	03:55:27.96	+09:43:44.4	21.99	1.30	22.36	1.11	0.20	5	14
40	uim0i	4	743.6	705.1	03:55:31.60	+09:45:08.8	20.17	1.34	17.72	1.43	0.10	0	13
41	uim0i	4	309.9	730.7	03:55:33.92	+09:44:43.0	20.47	1.81	19.00	0.00	0.61	1	16
42	uim0i	4	472.1	343.3	03:55:31.40	+09:44:24.2	20.92	0.91	20.85	1.09	0.73	4	17
43	uim0i	4	402.1	270.3	03:55:31.44	+09:44:14.1	21.47	1.57	19.79	1.87	0.73	4	14
44	uim0i	4	537.2	226.4	03:55:30.56	+09:44:19.5	21.93	1.15	21.97	1.24	0.13	5	15
45	uop0i	2	552.8	753.7	07:50:45.29	+14:39:21.8	21.02	1.66	18.62	1.66	0.08	0	13
46	uop0i	2	196.2	261.2	07:50:46.97	+14:40:17.0	21.39	0.59	20.47	0.81	0.23	3	15
47	uop0i	2	160.8	219.8	07:50:47.09	+14:40:22.0	21.80	1.59	19.55	1.30	0.04	0	13
48	uop0i	2	81.6	404.9	07:50:45.73	+14:40:19.5	21.96	1.38	19.70	1.03	0.07	0	12
49	uop0i	2	397.1	329.6	07:50:47.25	+14:39:56.3	21.99	1.02	20.78	1.01	0.61	3	13
50	uop0i	3	651.1	754.4	07:50:41.79	+14:41:11.3	20.58	0.69	20.52	0.83	0.40	3	17
51	uop0i	3	106.3	429.2	07:50:46.12	+14:41:10.4	20.96	2.07	18.53	2.04	0.62	0	13
52	uop0i	3	680.9	390.8	07:50:42.84	+14:40:38.7	21.10	0.50	20.93	0.00	0.71	4	15
53	uop0i	3	483.0	405.5	07:50:43.96	+14:40:49.8	21.43	0.96	18.89	1.29	0.02	0	13
54	uop0i	3	161.8	183.5	07:50:46.62	+14:40:46.6	21.46	0.75	22.03	1.12	0.48	5	15
55	uop0i	3	764.3	341.5	07:50:42.52	+14:40:30.4	21.36	0.64	21.01	0.68	0.58	4	15
56	uop0i	3	132.7	656.0	07:50:45.19	+14:41:28.5	21.88	0.51	19.68	0.41	0.17	0	13
57	uop0i	3	265.7	89.4	07:50:46.33	+14:40:33.3	21.74	1.09	20.63	0.91	0.65	2	14
58	uop0i	3	677.8	136.6	07:50:43.73	+14:40:17.1	21.92	0.60	21.08	0.47	0.67	3	14
59	uop0i	3	220.9	580.6	07:50:44.92	+14:41:17.8	21.70	1.62	20.93	1.94	0.14	4	14
60	uop0i	4	587.9	710.1	07:50:49.99	+14:42:00.4	20.38	2.02	18.18	1.88	0.03	0	13
61	uop0i	4	162.9	653.3	07:50:51.07	+14:41:20.9	20.58	0.50	19.77	0.59	0.37	1	15
62	uop0i	4	235.8	393.6	07:50:49.29	+14:41:14.6	20.77	1.03	18.15	0.97	0.14	0	13
63	uop0i	4	542.6	704.2	07:50:50.10	+14:41:56.2	20.80	1.69	18.41	1.80	0.22	0	13
64	uop0i	4	617.1	213.9	07:50:46.93	+14:41:38.8	21.18	0.45	19.97	0.36	0.09	1	15
65	uop0i	4	175.1	486.7	07:50:50.05	+14:41:13.9	21.17	1.39	21.00	1.47	0.33	6	15
66	uop0i	4	340.1	437.7	07:50:49.20	+14:41:25.7	21.83	1.99	19.40	1.57	0.14	0	13
67	uop0i	4	197.9	461.2	07:50:49.81	+14:41:14.6	21.83	2.05	19.40	1.79	0.69	0	13
68	uop0i	4	222.3	430.9	07:50:49.55	+14:41:15.2	21.78	0.94	21.32	1.00	0.31	4	14
69	uop0i	4	450.7	423.9	07:50:48.74	+14:41:34.7	21.59	1.84	20.67	1.90	0.30	2	14
70	uop0i	4	450.3	113.4	07:50:46.89	+14:41:19.4	21.88	0.83	20.68	0.74	0.30	2	13
71	uop0i	4	183.0	298.4	07:50:48.89	+14:41:05.3	21.80	1.55	21.51	1.54	0.72	4	14
72	usa2i	2	418.7	210.6	17:12:20.65	+33:35:15.7	20.83	0.71	18.40	0.60	0.02	0	14
73	usa2i	2	166.3	244.0	17:12:21.40	+33:35:39.2	21.15	0.83	00.00	0.00	0.67	6	17
74	usa2i	2	277.6	377.3	17:12:20.05	+33:35:36.1	21.30	1.16	21.33	1.14	0.14	6	18
75	usa2i	2	171.9	185.3	17:12:21.79	+33:35:35.8	21.90	1.91	19.31	2.05	0.05	0	13
76	usa2i	2	434.7	205.0	17:12:20.63	+33:35:14.1	21.98	1.63	19.51	1.70	0.24	0	13
77	usa2i	2	143.6	522.8	17:12:19.56	+33:35:54.7	21.99	0.81	21.81	1.01	0.59	3	16
78	usa2i	3	461.4	91.5	17:12:20.59	+33:36:03.6	20.85	2.31	18.42	2.16	0.13	0	14
79	usa2i	3	306.5	516.6	17:12:23.33	+33:36:32.6	21.40	1.89	18.95	1.74	0.49	0	13

TABLE 2—*Continued*

ID (1)	Field (2)	Chip (3)	X (4)	Y (5)	RA(J2000) (6)	DEC(J2000) (7)	I (8)	V-I (9)	Ic (10)	(V-I)c (11)	e (12)	T (13)	ApRad (14)
80	usa2i	3	464.4	242.8	17:12:21.16	+33:36:16.7	21.43	0.22	22.14	0.42	0.19	5	18
81	usa2i	3	458.0	202.6	17:12:21.05	+33:36:13.0	21.55	1.50	19.20	1.79	0.26	0	13
82	usa2i	3	575.7	88.7	17:12:19.79	+33:36:09.0	21.44	1.50	20.64	1.37	0.20	1	17
83	usa2i	3	439.3	85.3	17:12:20.72	+33:36:01.9	21.51	0.81	21.07	0.86	0.27	6	17
84	usa2i	3	520.5	270.8	17:12:20.88	+33:36:21.9	21.65	1.71	20.80	1.90	0.25	3	16
85	usa2i	4	292.9	149.9	17:12:25.06	+33:35:54.7	20.61	1.97	18.43	1.73	0.00	0	14
86	usa2i	4	396.0	389.9	17:12:27.12	+33:35:51.5	20.61	1.20	20.76	1.11	0.18	5	19
87	usa2i	4	239.7	704.9	17:12:28.66	+33:35:22.4	20.65	0.45	21.44	0.54	0.66	4	23
88	usa2i	4	258.0	495.7	17:12:27.30	+33:35:34.4	20.67	2.01	18.15	2.13	0.80	0	15
89	usa2i	4	642.4	290.4	17:12:27.42	+33:36:17.6	20.70	0.45	18.23	0.30	0.09	0	14
90	usa2i	4	77.5	264.9	17:12:24.99	+33:35:30.6	21.10	1.03	18.70	1.15	0.10	0	13
91	usa2i	4	466.0	330.4	17:12:26.99	+33:36:00.5	21.12	0.88	19.86	0.68	0.29	1	15
92	usa2i	4	377.5	484.0	17:12:27.70	+33:35:45.2	21.33	0.34	18.83	0.60	0.01	0	13
93	usa2i	4	281.3	576.5	17:12:27.95	+33:35:32.3	21.36	0.66	20.59	0.58	0.53	2	16
94	usa2i	4	762.3	638.5	17:12:30.29	+33:36:10.3	21.51	1.09	21.18	1.38	0.61	4	16
95	usa2i	4	505.8	729.6	17:12:29.89	+33:35:43.9	21.72	0.92	21.41	1.06	0.57	5	16
96	usa2i	4	571.1	261.9	17:12:26.95	+33:36:12.9	21.79	1.07	19.56	0.76	0.08	0	13
97	usa2i	4	733.7	219.8	17:12:27.31	+33:36:28.9	21.93	1.47	19.52	1.70	0.08	0	13
98	usa2i	4	578.6	530.3	17:12:28.82	+33:36:00.2	21.97	1.06	22.24	1.12	0.68	5	16
99	ux40i	2	460.0	174.0	15:19:39.63	+23:52:49.6	20.02	1.39	17.69	1.43	0.04	0	15
100	ux40i	2	139.1	607.9	15:19:43.53	+23:52:47.4	20.07	0.47	20.42	0.56	0.60	5	19
101	ux40i	2	150.0	553.8	15:19:43.17	+23:52:45.3	20.10	0.62	20.05	0.58	0.35	3	22
102	ux40i	2	101.3	668.4	15:19:44.04	+23:52:47.6	20.78	0.82	19.45	0.80	0.06	1	17
103	ux40i	2	475.8	703.1	15:19:42.74	+23:53:20.3	21.02	0.85	19.81	0.82	0.43	1	16
104	ux40i	2	262.6	157.2	15:19:40.33	+23:52:32.4	21.54	0.58	21.34	0.55	0.68	6	17
105	ux40i	2	503.3	516.1	15:19:41.51	+23:53:12.2	21.44	1.32	21.62	1.90	0.34	4	18
106	ux40i	2	725.6	221.7	15:19:38.85	+23:53:14.1	21.64	1.52	21.31	1.51	0.67	3	16
107	ux40i	2	177.0	147.5	15:19:40.62	+23:52:24.9	21.97	1.83	20.34	1.93	0.15	1	14
108	ux40i	3	726.8	618.0	15:19:46.87	+23:51:58.9	21.09	0.79	18.83	0.77	0.13	0	14
109	ux40i	3	735.9	733.1	15:19:47.38	+23:51:49.9	21.60	0.72	19.45	0.54	0.29	0	13
110	ux40i	3	417.3	244.3	15:19:43.51	+23:52:12.6	21.68	0.50	19.40	0.46	0.56	0	14
111	ux40i	3	229.4	313.7	15:19:42.66	+23:51:56.5	21.76	1.29	20.45	1.25	0.17	1	15
112	ux40i	3	78.1	735.1	15:19:43.45	+23:51:13.7	21.86	0.89	19.49	0.84	0.18	0	13
113	ux40i	3	217.2	504.7	15:19:43.35	+23:51:40.0	21.89	1.15	22.05	1.37	0.53	5	16
114	ux40i	4	290.8	635.1	15:19:37.82	+23:51:15.2	20.31	1.56	18.14	1.52	0.04	0	14
115	ux40i	4	199.3	477.6	15:19:38.41	+23:51:31.4	20.63	0.63	20.62	0.69	0.75	3	18
116	ux40i	4	136.3	566.5	15:19:37.62	+23:51:31.8	21.28	2.28	18.87	2.14	0.65	0	13
117	ux40i	4	626.3	259.6	15:19:41.42	+23:51:07.8	21.45	1.18	20.80	1.32	0.72	2	15
118	ux40i	4	151.6	376.5	15:19:38.83	+23:51:40.8	21.41	0.81	21.22	0.72	0.15	2	16
119	ux40i	4	524.2	584.9	15:19:39.05	+23:50:58.6	21.75	1.59	19.37	1.55	0.07	0	13
120	ux40i	4	418.0	240.2	15:19:40.72	+23:51:26.2	21.87	0.26	19.34	0.21	0.08	0	13
121	ux40i	4	486.1	504.1	15:19:39.39	+23:51:06.2	21.76	0.78	20.28	0.64	0.39	1	15
122	ux40i	4	457.6	520.1	15:19:39.18	+23:51:07.6	21.87	0.86	22.19	0.57	0.68	5	15
123	uy40i	2	276.2	434.5	14:35:15.58	+24:59:36.1	20.29	1.38	18.54	1.48	0.56	1	16
124	uy40i	2	647.8	120.3	14:35:12.31	+24:59:17.4	20.69	1.67	18.29	1.61	0.06	0	14
125	uy40i	2	399.7	579.3	14:35:15.03	+24:59:53.4	21.23	1.15	18.75	1.26	0.73	0	13
126	uy40i	2	450.5	347.1	14:35:14.17	+24:59:32.9	21.65	0.92	21.45	1.00	0.50	5	15
127	uy40i	2	209.4	404.5	14:35:15.98	+24:59:31.3	21.67	1.34	20.15	1.24	0.14	1	14
128	uy40i	2	257.6	423.8	14:35:15.68	+24:59:34.5	21.97	0.67	21.07	0.70	0.56	6	15
129	uy40i	2	245.7	202.2	14:35:15.28	+24:59:13.1	21.89	1.15	22.55	1.33	0.20	5	15
130	uy40i	3	396.0	192.8	14:35:17.38	+24:59:23.6	20.29	0.65	20.86	0.73	0.95	4	22
131	uy40i	3	754.0	309.3	14:35:18.99	+24:59:53.9	20.48	0.51	20.74	0.77	0.56	3	19
132	uy40i	3	467.2	587.0	14:35:20.28	+24:59:18.4	20.91	1.12	18.51	1.11	0.08	0	13
133	uy40i	3	502.9	354.9	14:35:18.74	+24:59:28.8	21.08	1.04	20.91	0.89	0.82	3	17
134	uy40i	3	729.1	666.0	14:35:21.40	+24:59:40.7	21.45	2.82	00.00	0.00	0.07	0	13
135	uy40i	3	209.3	117.8	14:35:16.45	+24:59:08.2	21.38	1.23	20.36	1.31	0.25	1	15
136	uy40i	3	229.0	360.1	14:35:18.17	+24:59:02.7	21.38	1.39	20.98	1.59	0.44	4	17
137	uy40i	3	173.9	347.6	14:35:17.96	+24:58:57.9	21.71	1.28	20.52	1.41	0.43	1	14
138	uy40i	3	90.2	430.6	14:35:18.36	+24:58:47.5	21.63	1.34	21.80	1.58	0.81	4	16
139	uy40i	3	481.5	741.4	14:35:21.38	+24:59:15.2	21.84	0.48	20.58	0.38	0.87	1	14
140	uy40i	3	660.9	90.4	14:35:17.26	+24:59:51.6	21.94	1.65	20.13	1.64	0.16	0	13
141	uy40i	3	175.6	584.5	14:35:19.62	+24:58:50.9	21.99	1.58	20.91	2.22	0.13	3	14
142	uy40i	4	198.3	388.1	14:35:16.11	+24:58:27.9	21.13	0.99	18.62	0.91	0.31	0	13
143	uy40i	4	471.7	188.2	14:35:18.43	+24:58:36.6	21.62	0.66	20.21	0.68	0.04	1	14
144	uy40i	4	542.1	180.6	14:35:18.93	+24:58:35.0	21.62	1.82	20.46	1.96	0.12	1	15

NOTE.—Col. (1): Object ID.
Col. (2): MDS field name.
Col. (3): WFPC2 CCD number: 1 = PC, 2, 3, 4 = WFC.
Col. (4): Original X pixel position on the WFPC2 CCD.
Col. (5): Original Y pixel position on the WFPC2 CCD.
Cols. (6)–(7): Right ascension and declination of the object in J2000.00 coordinates. Relative R.A.s and decl.'s should be accurate to within 0".1. Absolute WFPC2 astrometry is only accurate to ~0".5–1".
Col. (8): Total I_{814} magnitude.
Col. (9): Total $(V-I)$ color.
Col. (10): Central I-band surface brightness within a radius of 0".2.
Col. (11): Central $(V-I)$ color within a radius of 0".2.
Col. (12): Image ellipticity $e = 1 - a/b$, computed from the outermost isophote.
Col. (13): Galaxy type: 0 = E, 1 = Sa, 2 = Sb, 3 = Sc, 4 = Sd, 5 = Irr, 6 = peculiar.
Col. (14): Aperture radius in pixels used to determine the I-band magnitude.

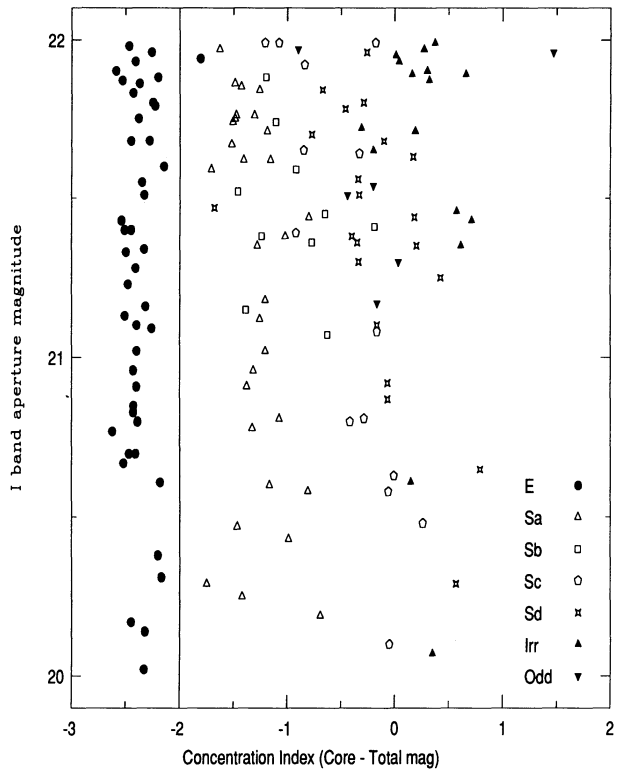

FIG. 3.—A comparison between the morphological classification and the concentration of a galaxy's light. The concentration index (C.I.) is the apparent central SB or core aperture magnitude minus the total magnitude. A low value of the C.I. suggests that the majority of the light is concentrated toward the center. The ellipticals form a clearly distinct population, but the late-type galaxies are less well distinguished by this method, as expected.

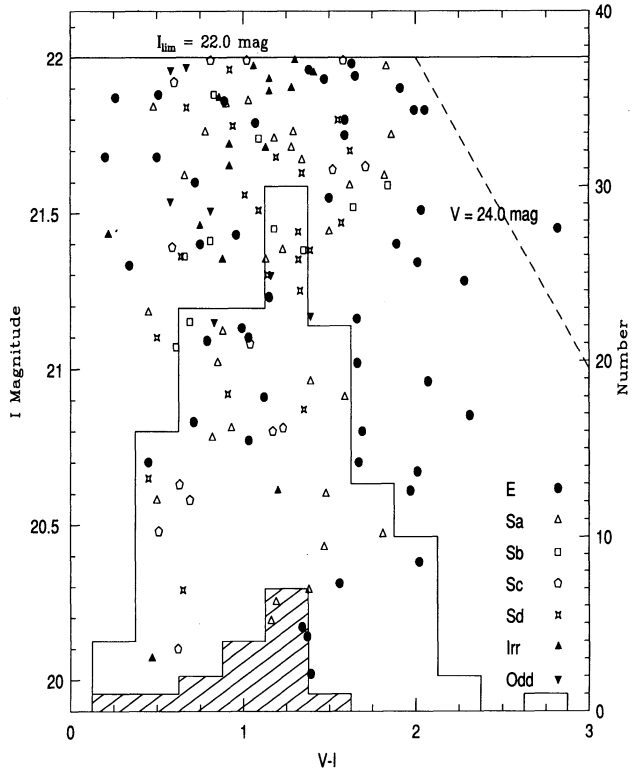

FIG. 4.—The $(V-I)$ color for the sample shows little or no trend with apparent I-band magnitude or morphological type, although few irregulars and late-type galaxies are seen with colors redder than $(V-I) = 1.5$. Note the nonnegligible fraction of *blue* galaxies classified as E/S0 which have $r^{1/4}$ light profiles. Also shown is the histogram of the $(V-I)$ data for the entire sample and for the irregulars alone (*shaded area*).

4. GLOBAL PROPERTIES OF THE LATE-TYPE *HST* GALAXIES

Without complete redshift information, we cannot distinguish between genuine irregular galaxies of low intrinsic luminosity at lower redshifts and normal galaxies which have developed an irregular appearance, perhaps due to merging or a violent asymmetric burst of star formation at moderate to large redshifts. The rather low mean redshifts observed in the field galaxy redshift surveys down to $B_J \simeq 23.5$ mag (BES; Colless et al. 1990, 1991, 1993; Cowie et al. 1991; Lilly et al. 1991) imply that only limited luminosity evolution can have occurred in the intrinsically brighter galaxy populations. Hence, those galaxies with a highly irregular appearance are more likely to be intrinsically low-luminosity systems with inherent irregular morphology, or intrinsically low-luminosity systems undergoing some evolutionary process, or a combination thereof. For the purposes of this paper, however, we exclude the "peculiar" galaxies and consider only the ellipticals and early- and late-type spirals plus what we believe to be the genuine irregulars based primarily on their low apparent central SB and flat light profiles. The mean apparent central SB for each of these types is $\mu_I^{\rm E} = 18.5 \pm 0.2$, $\mu_I^{\rm Sa} = 19.9 \pm 0.2$, $\mu_I^{\rm Sb} = 20.5 \pm 0.2$, $\mu_I^{\rm Sc} = 20.8 \pm 0.3$, $\mu_I^{\rm Sd} = 21.2 \pm 0.3$, and $\mu_I^{\rm Irr} = 21.8 \pm 0.2$ mag arcsec^{-2}. Note that our central SB was measured as the core SB within the central (0.″2) ellipse from the RGASP PROF package (Cawson 1983). Quoted rms errors are based on the number of objects binned into each group.

Figure 4 shows the integrated $(V-I)$ color versus magnitude for the full sample with the equivalent histogram overlain. There is little or no distinct trend in color with apparent magnitude *or* with morphological type. This is mainly a result of the rather small wavelength baseline between the F606W and F814W filters (which, however, overlap little in wavelength). *No* irregulars are seen with colors redder than $(V-I) \simeq 1.5$ mag, and *no* spirals exhibit colors redder than $(V-I) \simeq 2.0$ mag. The shaded area shows the distribution of irregulars only and is not found to be significantly bluer than that of the overall sample [$(V-I) = 1.2 \pm 0.1$ mag]. For each individual type, the observed mean colors are $(V-I)_{\rm E} = 1.4 \pm 0.2$, $(V-I)_{\rm Sa} = 1.2 \pm 0.2$, $(V-I)_{\rm Sb} = 1.1 \pm 0.2$, $(V-I)_{\rm Sc} = 1.0 \pm 0.3$, $(V-I)_{\rm Sd} = 1.1 \pm 0.3$ and $(V-I)_{\rm Irr} = 1.0 \pm 0.2$ mag.

Note that the mean color for the entire sample agrees well with that determined by GR94b when converted to a common filter system (Bahcall et al. 1994). Figure 5 shows the predicted color versus redshift for the various galaxy types. The local colors for each Hubble type were taken from the models in Windhorst et al. (1994b): $(V-I)_{\rm E/S0} \simeq 1.4 \pm 0.2$, $(V-I)_{\rm Sabc} \simeq 1.1 \pm 0.2$, and $(V-I)_{\rm Sd/Irr} \simeq 1.0 \pm 0.2$ mag. K-corrections for galaxy types E/S0, Sa, Sb, Sc, and Sd/Irr were derived from the present day spectra of Guiderdoni & Rocca-Volmerange (1987, 1988) for the WFPC2 V_{606} and I_{814} filters (M. Im 1995, private communication). Based on their likely zero-redshift spectral energy distributions (SEDs), the Hubble classes are expected to have a *range* in observed $(V-I)$ color of $0.9 < (V-I)_{\rm E/S0} < 2.7$, $0.7 < (V-I)_{\rm Sabc} < 2.2$, and $0.3 < (V-I)_{\rm Sd/Irr} < 1.8$ mag, depending on their exact redshift distribution. Our observed $(V-I)$ color range is generally consistent with these expecta-

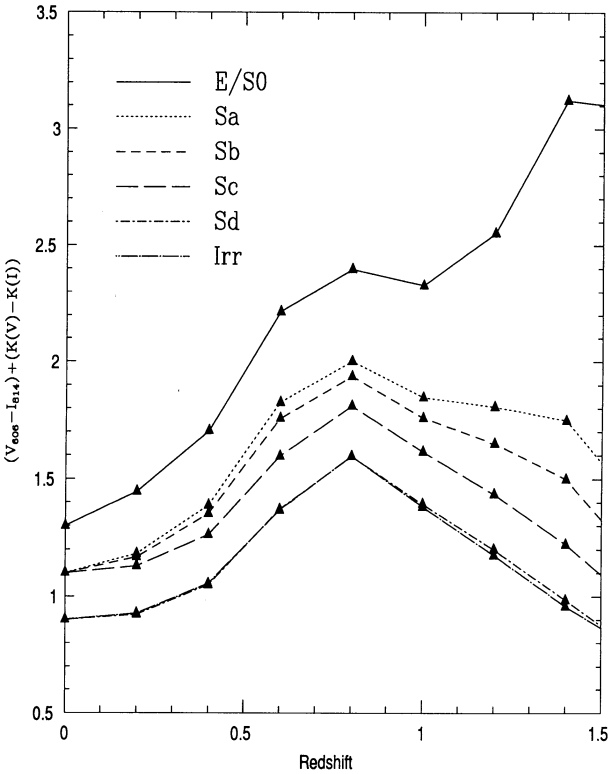

FIG. 5.—The expected relation between color and redshift for the Hubble sequence, assuming no-evolution, but using simple K-corrections derived from the present-day spectra of Guiderdoni & Rocca-Volmerange (1987, 1988) for the WFPC2 V_{606} and I_{814} filters (M. Im 1995, private communication).

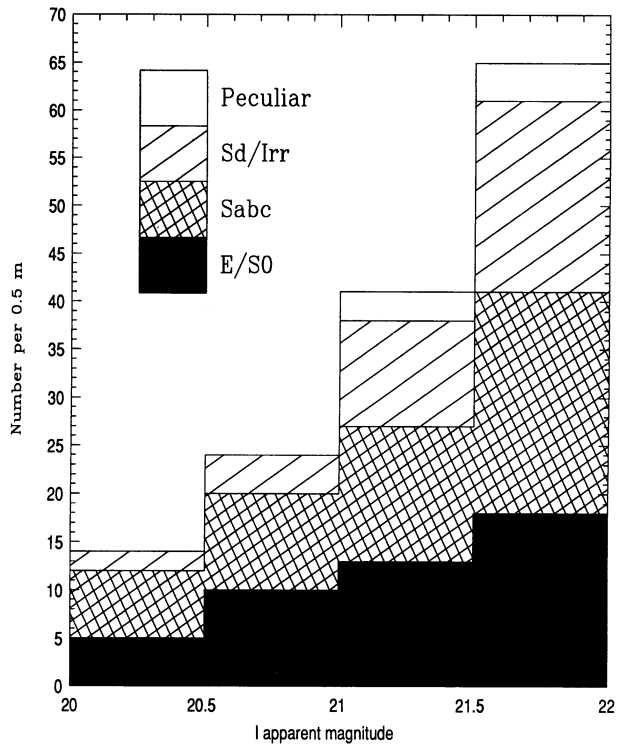

FIG. 6.—The number of galaxies observed for each type as a function of I-band magnitude. This shows a rapid increase in the number of irregular galaxies over the conventional spirals and ellipticals. The initial mix of 36% E, 50% Sabc, and 14% Sd/Irr at $m_I = 20.25$ mag becomes 28% E, 35% Sabc, and 31% Sd/Irr at $m_I = 21.75$ mag. Typical errors in these percentages are ~5%–8%. If this trend continues, then late-types and irregulars will make up the bulk of the galaxy population observed at fainter magnitudes (see Driver et al. 1995a).

tions: the only major exception is the surprising abundance of very blue E/S0's with $(V-I) \lesssim 1$ mag. This may imply an error in our method of classifications (i.e., a preponderance of blue compact dwarf systems or perhaps faint stars misclassified as E/S0's), or that the E/S0 population has evolved (Charlot & Bruzual 1991), and/or a strong color-luminosity relation for E/S0 galaxies. Blue E/S0 systems are known to exist in other samples studied with *HST* (e.g., compact narrow emission-line galaxies; see Koo et al. 1995, see also Im et al. 1995b) but are not normally noted in significant numbers in ground-based field surveys. However, they could have been missed as E/S0's in typical ground-based seeing. Our sample of E/S0's has a preponderance of $r^{1/4}$ light profiles, even though a non-negligible fraction has rather small scale lengths ($r_e \lesssim 0''.3$, CRGINOW). A spectroscopic follow-up is needed to reveal the nature of these blue E/S0 classifications.

Figure 6 shows the change in morphological mix from the bright to the faint end of our magnitude range and shows a distinct increase in the *ratio* of late-type galaxies to bright spirals plus ellipticals. The percentage mix changes from 36% E/S0, 50% Sabc, 14% Sd/Irr at $m_I = 20.25$ mag to 28% E/S0, 35% Sabc, and 31% Sd/Irr at $m_I = 21.75$ mag (+6% peculiar). There is thus a rapid increase in the number of galaxies with late-type morphology toward progressively fainter magnitudes. Our high-resolution *HST* images thus confirm the initial claims that late-type galaxies are responsible for the excess of faint blue objects observed in deep CCD surveys (see § 1). The bright end of our sample compares well to that observed by Shanks et al. (1984), who found 43% E/S0, 45% Sabc, and 12% Sd/Irr. Note that galaxies classified as peculiar (i.e., obvious mergers or images with a bright core coupled with irregular structure) also become more prevalent at fainter magnitudes. This may be a reflection of the increasing volume surveyed at fainter magnitudes making the catalog more complete for rarer types. Alternatively, it could represent an epoch at which brighter field galaxies merged more frequently (Burkey et al. 1994). Clearly, with only seven galaxies it is impossible to draw substantial conclusions for the peculiar types other than that they *may* represent evolution in a *small fraction* (seven of ~110) of the brighter field population, which *appears* to become more frequent at fainter magnitudes.

5. THE MORPHOLOGICAL GALAXY COUNTS OBSERVED WITH *HST*

5.1. *The Observed Counts as a Function of Galaxy Type*

Figure 7 shows the more conventional differential galaxy number counts versus I-band magnitude plots for (*a*) the total galaxy sample; (*b*) the elliptical/compact galaxies (E/S0's); (*c*) spiral galaxies (Sabc's); and (*d*) late-type galaxies (Sd/Irr). The counts of the total sample are linear, suggesting that the sample is indeed representative and complete down to at least $I = 22$ mag, as inferred from Figure 1. However, the slope is slightly steeper (0.43 ± 0.05) than that observed by other groups in the I band (Tyson 1988; Driver et al. 1994; Burkey et al. 1994; Neuschaefer & Windhorst 1995). This may suggest that the ground-based samples suffer from partial incompleteness or star-galaxy confusion (Neuschaefer & Windhorst 1995; CRGINOW), or more likely that the discrepancy is a reflection

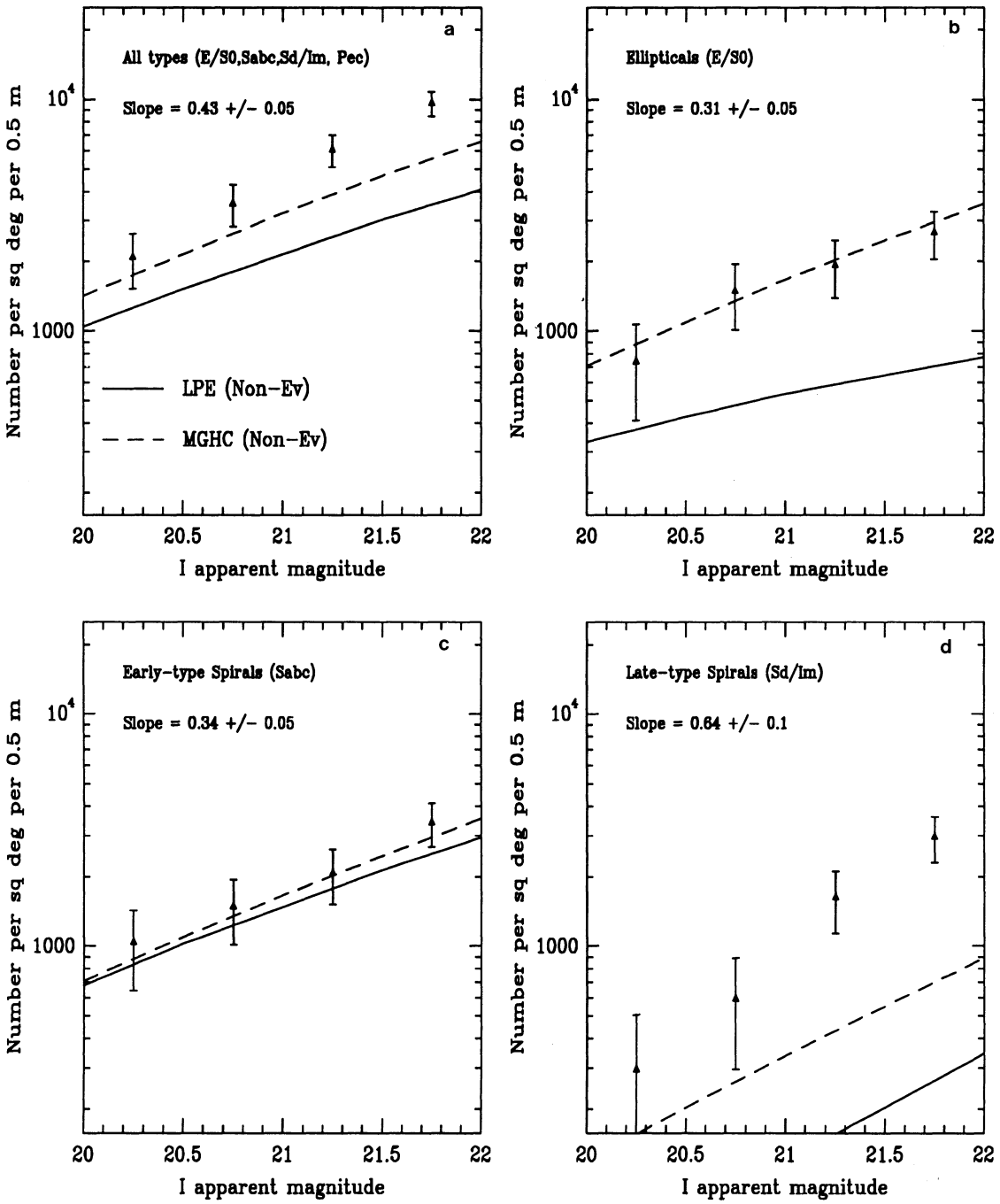

FIG. 7.—Differential galaxy number counts for (*a*) our complete *HST* sample; (*b*) E/S0 galaxies; (*c*) Sabc galaxies; and (*d*) late-type galaxies (Sd/Irr). The slope of the overall counts is consistent with data from other groups (see Fig. 8) and implies that our sample is complete at least down to $I = 22.0$ mag. The ellipticals and spirals (*b*, *c*) have shallower slopes. The model predictions are for an LPEM LF model (*solid lines*) and on MGHC LF model (*dashed lines*). For (*b*) and (*c*), the MGHC LF models agree well with our observed *HST* counts using no-evolution and a standard cosmology. However, the late-type galaxies follow a much steeper slope, indicating that either they are more local and less affected by cosmology, and/or that they are undergoing a significant amount of evolution. The model lines are assuming two alternate luminosity functions and no-evolution.

of the limited magnitude range covered by our high S/N sample (the ground-based slopes are typically measured out to fainter magnitudes, where the counts are expected to flatten). The individual counts of ellipticals (E/S0's; Fig. 7*b*) and early-type spirals (Sabc's; Fig. 7*c*) have flatter and comparable slopes of 0.31 ± 0.05 and 0.34 ± 0.05, respectively. The counts of the late-type galaxies, however, exhibit a much steeper and rather unexpected slope of 0.64 ± 0.1 (Fig. 7*d*), consistent with the Euclidean value. GL95a independently find a similar trend for the fractions of morphological types over a comparable magnitude range. We conclude that the steep number counts of the late-type/irregular population likely give rise to the faint blue galaxies observed at faint magnitudes. If this trend continues, this implies that the faint galaxy number counts (and the extra-

galactic background light) are largely if not entirely dominated by late-type galaxies. Are these late-type/irregulars expected, are they evolving, and if so, through what mechanism?

5.2. *Modeling the Morphological Galaxy Counts*

To compare these observations to a series of model predictions, we must adopt a parameterization of the *local* space density of galaxies for each type, a cosmological model, and quantify any evolutionary processes (Driver et al. 1994). The local space density of galaxies is typically represented by a Schechter (1976) luminosity function (LF), which is derived from a local redshift survey down to some specified magnitude limit.[4] Two of the most recent local redshift surveys are those by Loveday et al. (1992, hereafter LPEM) and Marzke et al. (1994b, hereafter MGHC). They find significantly different Schechter parameters for the LF of the local populations. Table 3 shows the Schechter parameters derived from these surveys corresponding to the range of galaxy types adopted in this paper (i.e., E/S0, Sabc, Sd/Irr).

Parameters for the LPEM LF, listed in Table 3, were derived as follows: M_* and α for E/S0's and Sabc's come directly from their tabulated LFs for early- and late-type galaxies. The ϕ_* values were measured from Figure 3 of LPEM. Since LPEM do not segregate the early-type and late-type spirals, we divide the population arbitrarily by absolute magnitude, assuming galaxies brighter than $M_B = -18$ are Sabc, and those fainter are Sd/Irr (see Binggeli, Sandage, & Tammann 1988). Hence, the Sabc LF is truncated (via an exponential cutoff, i.e., $\exp[-10^{0.4(M-M^{\rm Cut})}]$) at $M^{\rm Cut} = -18.0$ and $M_* = -18.0$ is adopted for Sd/Irr's. The slope and normalization for the Sd/Irr's was then chosen such that the (Sabc + Sd/Irr) LF is consistent with the (Sp/Irr) LF shown in Figure 3 of LPEM. Parameters for the MGHC LF were taken as the average between the appropriate classes listed in their Table 1 (as suggested by R. Marzke 1995, private communication). However, note that the ϕ_* for the total LF (i.e., summed over all types) listed in Marzke et al. (1995a) is twice that quoted in MGHC and, if correct, would alleviate the requirement to renormalize the models at $b_J = 18$ mag (see § 5.3).

Table 3 shows that the level of discrepancy between these two local surveys is substantial. Hence, for the sake of completeness we shall use both sets of parameters. The cosmology we adopt is a standard Einstein–de Sitter model with $\Lambda = 0$, $\Omega = 1$, $q_0 = 0.5$, and we also adopt $H_0 = 50$ km s^{-1} Mpc^{-1}. K-corrections for galaxy types E/S0, Sa, Sb, Sc, and Sd/Irr were derived in § 4. Since our main aim is to find any evolution that may have occurred for each morphological type, we shall assume no evolution in the model predictions. To convert the B-band Schechter parameters to the I-band, we adopt $(B-I)_{\rm E/S0} = 2.3$ mag, $(B-I)_{\rm Sabc} = 1.9$ mag, and $(B-I)_{\rm Sd/Irr} = 1.4$ mag (from the models in Windhorst et al. 1994b).

5.3. *The Problem of LF Normalization in Models*

An additional problem with faint galaxy models is the question of the magnitude at which to normalize the LF predictions to the observations. The optimal normalization is done at a flux level at which the mean galaxy distance is sufficiently large that a homogeneous volume is sampled, but not so large that significant evolution has already taken place. Simply adopting the normalizations derived from the *local* redshift surveys results in a severe underestimation of the observed galaxy counts already at relatively low redshift, where little evolution is expected. This reflects the faster than Euclidean rise of the observed number counts at bright magnitudes (Shanks 1989). Either strong evolution must be occurring locally (Maddox et al. 1990), or the local redshift surveys are incomplete for galaxies of dwarflike luminosities (Ferguson & McGaugh 1995), or our location in the universe is unusually sparse (e.g., due to large-scale structure, etc.),[5] or a combination thereof. Which of these factors is responsible is not known (see Shanks 1989 for a review).

TABLE 3

SCHECHTER FUNCTION PARAMETERS FOR THE LFS OF DIFFERENT GALAXY CLASSES

Survey	Type	M_*	α	ϕ_*
LPEM.....	E/S0	−21.2	+0.2	4.00×10^{-4}
	Sabc	−20.9	−0.8	1.00×10^{-3}
	Sd/Irr	−18.5	−1.1	7.00×10^{-4}
MGHC.....	E/S0	−20.5	−0.9	1.14×10^{-3}
	Sabc	−20.3	−0.8	1.74×10^{-3}
	Sd/Irr	−20.3	−1.5	2.50×10^{-4}

Figure 8 illustrates the errors associated with faint galaxy models resulting from this normalization problem. Figure 8 compares the unnormalized no-evolution predictions derived from the two sets of Schechter function parameters listed in Table 3. Both models underpredict the counts for $m_{B_J} \simeq 16$ mag, and the predictions extrapolated to fainter magnitudes differ even more significantly from our *HST* data. Traditionally, most faint galaxy models are normalized to the observations in the range $18 < m_{B_J} < 22$ mag (Shanks 1989), which alleviates a good fraction of the discrepancy between the models and observations at fainter magnitudes. The justification is that at $m_{B_J} \simeq 20.0$ mag even an $0.1L_*$ galaxy will be at a sufficiently large distance ($z > 0.1$; Koo & Kron 1992) that the sampled volume is likely homogeneous and isotropic, but not so great that evolutionary processes have likely already occurred. It is interesting to note that *if* the counts are normalized at $m_{B_J} \simeq 18$ mag, the no-evolution models *remain* in good agreement with the observations down to $m_{B_J} \simeq 22$ mag, where the median redshift is $z \sim 0.25$ (KK92). This suggests that we may indeed live in a sparse *local* region of space (for $m_{B_J} \lesssim 16$ mag) and is difficult to reconcile with a scenario of strong evolution at *low* redshifts (such evolution would then have to have switched off between $18 \lesssim m_{B_J} \lesssim 22$ mag, which is rather unlikely). The debate will continue as to the nature of this discrepancy, so here we will adopt the standard normalization at $m_{B_J} \simeq 18.0$ mag (which is valid until $m_{B_J} \simeq 22$ mag), as illustrated by the filled circle in Figure 8, and increase the ϕ_* values listed in Table 3 uniformly for all galaxy types by 0.3 dex. We do not mean to imply here that the local surveys are ~50% incomplete (although the Zwicky magnitudes may cause some problems at the faint end of the CfA survey), and we emphasize that there is likely a combination of causes for the normalization problem. A recent LF based on a nearby galaxy sample selected in the K band suggested a significantly larger ϕ_* value (Glazebrook et al. 1995c) than the optical values in Table 3.

[4] The problems associated with magnitude-limited surveys of this kind are discussed in further detail in Marzke, Huchra, & Geller (1994a) and Driver & Phillipps (1995).

[5] Note that if local space is underdense in galaxies, low-luminosity systems will be severely underrepresented in bright magnitude-limited surveys, because of the smaller volume over which they are seen (Driver & Phillipps 1995).

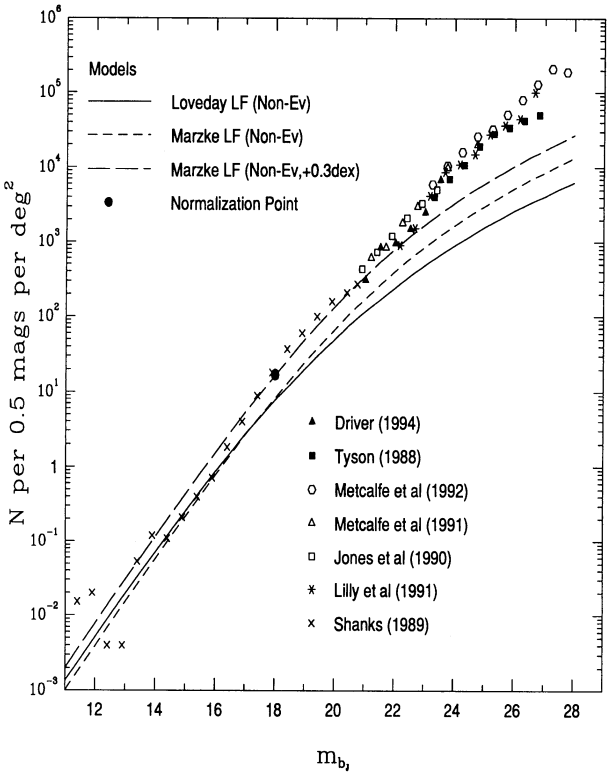

FIG. 8.—The differential galaxy number counts in the B_J band from various sources listed in the figure. The model lines show predictions using the *non-evolving* LPEM LF (*solid line*) and the MGHC LF (*small dashed line*). These model lines are unnormalized (i.e., as locally determined). Not only do the two models give dramatically different predictions at faint magnitudes, but also does neither model match the counts fainter than $m_{B_J} \simeq 17$ mag, suggesting local evolution, local selection effects, and/or a local inhomogeneity (see text). Most galaxy models are normalized to the counts at $18.0 < m_{B_J} < 22.0$ mag (cf. Shanks 1989; see § 5.2). Here we normalize at $m_{B_J} \simeq 18$ mag, as indicated by the single solid circle, which implies a 0.3 dex increase of the local LF. The *normalized* Marzke LF model is shown as a large dashed line.

We mention in this context additional constraints from the well-known source counts and the cosmological evolution of the radio source population (Windhorst 1984; Windhorst, Mathis, & Neuschaefer 1990; Windhorst et al. 1993; Condon 1989) on the LF normalization problem. The initial steep rise of the radio source counts at jansky levels (with a magnitude slope of ~ 0.72!) also suggests the presence of a "local hole" in the space density of at least radio galaxies, and their strong cosmological evolution is known not to start until $z \simeq 0.3$ (Windhorst 1984; Windhorst et al. 1990; Condon 1989). Hence, *if* field galaxies had the same space distribution as radio galaxies, LF normalization is suggested at $0.1 < z < 0.2$, consistent with our normalization at $z \simeq 0.15$. This argument is likely not valid for radio sources with 1.4 GHz fluxes $\gtrsim 10$ mJy, which undergo strong cosmological evolution and are *not* associated with field galaxies (Windhorst et al. 1990), but quite possibly valid for μJy radio sources which also undergo some cosmological evolution (Condon 1989), albeit not as strong and not until $z \gtrsim 0.3$, and merge into the general population of field galaxies at the sub-μJy level (Windhorst et al. 1993).

5.4. *Model Predictions for the Morphological HST Counts*

Figure 7 shows the model predictions from the LFs of LPEM and MGHC for each morphological type with the normalizations adopted in § 5.3. The LFs of LPEM and MGHC each suggest different amounts of evolution when compared to our *HST* data in Figure 7. The prediction based on the LPEM LF (*solid lines*) appears to suggest a large amount of evolution in the E/S0's and an inordinate amount of evolution in the late-type spirals. Alternatively, the MGHC model (*dashed lines*) implies that no evolution is required in the E/S0 and early-type spirals. LPEM and MGHC both note that the LPEM LF is incomplete for early-type galaxies at the higher redshifts in the LPEM sample, which could explain the large discrepancy between the two predictions for E/S0's. *If* true, then our *HST* data for E/S0's and Sabc's appear to be consistent with the no-evolution prediction of the MGHC LF [bearing in mind that the increased normalization of the models at $m_{B_J} \simeq 18$ mag ($m_I \simeq 16$) is still unexplained, although possible reasons are given above]. The dashed lines in Figure 7 represent the locally *normalized* predictions.

For late-type spirals/irregulars, the predictions are drastically different between the two models. This highlights the large uncertainty with which the *faint* end of the local field LF is known (Driver & Phillipps 1995) and how important this part of the LF is in faint galaxy models (Driver et al. 1994; Driver 1994). LPEM find a flat faint end slope $\alpha \simeq -1.0$, and MGHC find a much steeper slope $\alpha \simeq -1.5$. They actually find a slope of $\alpha \simeq -1.8$ for the Sm-Im types alone, so in Table 3 we have averaged the slopes found by MGHC for Sc-Sd and Sm-Im types to generate a realistic Sd-Im slope (R. Marzke 1995, private communication). Such a steepening of the faint end slope is mostly dominated by the late-type population (Binggeli, Sandage, & Tammann 1988; MGHC) and has been favored in many recent faint galaxy models (e.g., Koo & Kron 1992; Koo, Gronwall, & Bruzual 1993; Driver et al. 1994; Ferguson & McGaugh 1995; Phillipps & Driver 1995). However, these models typically remain inconsistent with the faint redshift surveys (e.g., Colless et al. 1990, 1991, 1993; BES; Cowie et al. 1991; Glazebrook et al. 1995b, and references therein).

The prediction based on an LPEM LF requires an increase in the galaxy number density at $m_I = 21.75$ of ~ 1 dex, while the prediction based on the MGHC LF requires ~ 0.5 dex. To obtain a crude estimate of the amount of evolution required, we can equate these number density increases to volume increases and calculate the magnitude limit of these additional volumes (assuming that galaxy numbers are preserved). The difference between this magnitude limit and that of our sample yields an estimate of the amount of *luminosity evolution* required in the *entire* population to match the observed counts [i.e., $N(m) \propto V(m) \propto L^{3/2} \Rightarrow \Delta m \propto (1/0.6) \log (V_2/V_1)$]. This yields luminosity increases of $\Delta m_{\rm LPEM} \sim 1.7$ and $\Delta m_{\rm MGHC} \sim 0.8$ mag.

The M_* value adopted for the LPEM late-type/irregulars would imply that objects with $m_I \sim 21.75$ are at $z \lesssim 0.4$ (or $\lesssim 6$ Gyr on look-back time). Over this timescale, a typical isolated starburst event will fade by $\simeq 1.8$ mag (see, e.g., Fig. 3 of Wyse 1985, which is based on a formation starburst within a rapidly condensing gas cloud). However, if there is a significant underlying population, the *total* fading of the *whole* galaxy's luminosity will change by considerably less, dependent on the luminosity ratio of the new to old populations ~ 6 Gyr after the new burst. The implication is that for a fading of $\Delta m \sim 1.8$, a global starburst is required with strength comparable to that of the galaxy's initial formation (or the sum of all previous starbursts). That such events have occurred in the *entire* late-

type/irregular population over the past 6 Gyr seems highly improbable, although we note that the star formation mechanisms of late-type galaxies are poorly known (see Hodge 1989, in which evidence for a wide range of star-forming timescales in local group members is discussed).

Alternatively, the MGHC-based model requires a luminosity evolution of $\Delta m \sim 1.8$, but only for $\sim 15\%$ of the population (from consideration of luminosity conservation). This would then imply that based on an MGHC-based model, we only require a major global starburst event in 15% of the late-type population over the past 6 Gyr. Of course, other evolutionary scenarios exist, but this crude calculation is indicative of the comparative amounts of evolution required to match the two local LF models to our *HST* observations.

Figure 9 shows the predicted *B*-band redshift distributions at $m_I \simeq 21.75$ mag ($\approx m_{B_J} \simeq 23.5$ mag), compared to the faint redshift surveys of Colless et al. (1993) and Glazebrook et al. (1995b). The predicted redshift distributions have been scaled up to match the observed distribution. (Note that this is somewhat misleading, since neither LF model matches the *B*-band number counts at this magnitude, but it is easier to compare the *rescaled* predictions to the *shape* of the observed redshift distribution). The form of the LPEM LF matches the overall distribution closely, while the MGHC LF both overpredicts the number of low redshift galaxies and underpredicts the number of high redshift galaxies. Given that luminosity evolution will shift the peak of the redshift distribution toward higher redshifts, and that some evolution is required to match the steep counts, then the distribution toward lower redshifts of the no-evolution MGHC LF is not unexpected. Of greater concern is the lack of $z > 0.5$ objects predicted by MGHC (as a result of the low M_*-values in their E/S0 and Sabc Schechter functions; see Table 3). The only way to simultaneously reconcile the redshift distribution and the morphological counts is through an evolutionary scenario in which the intrinsically *bright* late-type galaxies are undergoing evolution at $z \geq 0.5$. Such models are explored in more detail in Philipps & Driver (1995).

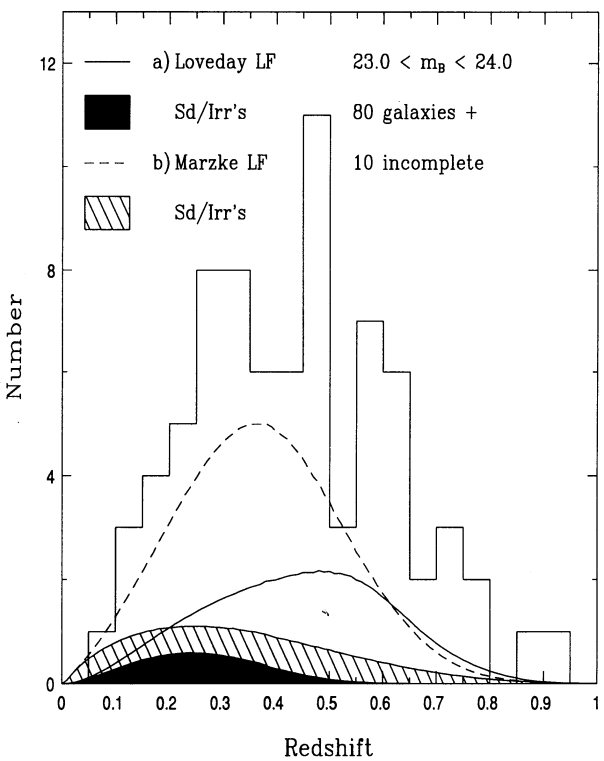

FIG. 9.—The predicted redshift distribution for $m_{B_J} = 23.5$ mag compared to the data of Colless et al. (1993) and Glazebrook et al. (1995b). The model distributions are scaled to reflect the discrepancy between the observed and predicted number counts at $m_I \sim 23.5$ mag. The shaded areas represent the contribution from the late-type/irregulars population.

6. THE MORPHOLOGY OF IRREGULAR GALAXIES IN THE *HST* SAMPLE

Figure 10 shows *V*- and *I*-band gray-scale images and contour plots for each of the 16 irregulars and the seven peculiar types, as described in the caption. Qualitatively, the majority of this sample is characterized by irregular shaped outer light profiles and, in many cases, a complex nucleus consisting of a number of higher SB regions. Objects 6, 18, 33, 38, 39, 44, 54, 80, 86, 95, 98, 100, 113, 122, and 126 represent the (15) genuine irregulars, and objects 29, 65, 73, 74, 83, 104, and 128 represent the (seven) "peculiar" galaxies. The irregulars appear to fall into two categories: (1) those which appear inert, and (2) those which contain multiple cores. Objects 6, 38, 44, 54, 113, and 126 are good examples of multiple-core objects and comprise about $\sim 40\%$ of the irregular sample. Such complex cores may imply active star formation, e.g., via spontaneous or merger-induced starbursts. Objects 86 and 100 appear to have strong core structure, but in reality this is a manifestation of their much brighter apparent magnitude. Their apparent central SB is significantly lower than that of other galaxies of comparable flux (cf. Table 2). Both galaxies also show some evidence of merging, but the central regions appear relatively undisturbed. Objects 54, 80, 122, and 126 also show evidence for a close companion which *may* be responsible for their multiple core structure. *If* a multiple core *is* indicative of currently ongoing starformation (i.e., evolution), then both spontaneous (i.e., no obvious merger) and merger-induced starbursts appear to occur. Nevertheless, half the irregular population (objects 18, 33, 39, 86, 95, 98, 100, 129) appears relatively inert with low SB cores and with extended irregular shaped light profiles. This suggests that *both* merger-induced evolution and/or active starbursts, *and* a higher than anticipated density of local dwarfs contribute to the faint blue galaxy excess at $m_I \simeq 22$ mag. The density of irregular galaxies *alone* (i.e., $\sim 50\%$ of the Sd/Irr population) appears to be inconsistent with the LPEM LF.

If all the "apparently evolving" galaxies (i.e., $\sim 50\%$) were removed from Figure 7*d*, this would reduce their observed surface density by *only* 0.3 dex, and our *HST* data would *still* remain inconsistent with the LPEM LF model by 0.7 dex! That is, not only is the LPEM LF model inconsistent with our full *HST* Sd/Irr sample, but it is also inconsistent with the inert-looking *HST* galaxies alone. Such evidence argues convincingly *for* an MGHC LF, where the faint end slope of the field LF is steeper ($\alpha \gtrsim 1.5$) than the often *asssumed* value (i.e., $\alpha \sim 1.0$). Hence, it appears that a combination of evolution and a steep faint end LF is responsible for the FBGs. The mode of evolution is still unclear, but both mergers and isolated systems with multiple cores are evident in roughly equal numbers in our *HST* images.

7. SUMMARY AND CONCLUSIONS

We presented a complete sample of 144 *HST*/WFPC2 field galaxies from the Medium Deep Survey in the magnitude

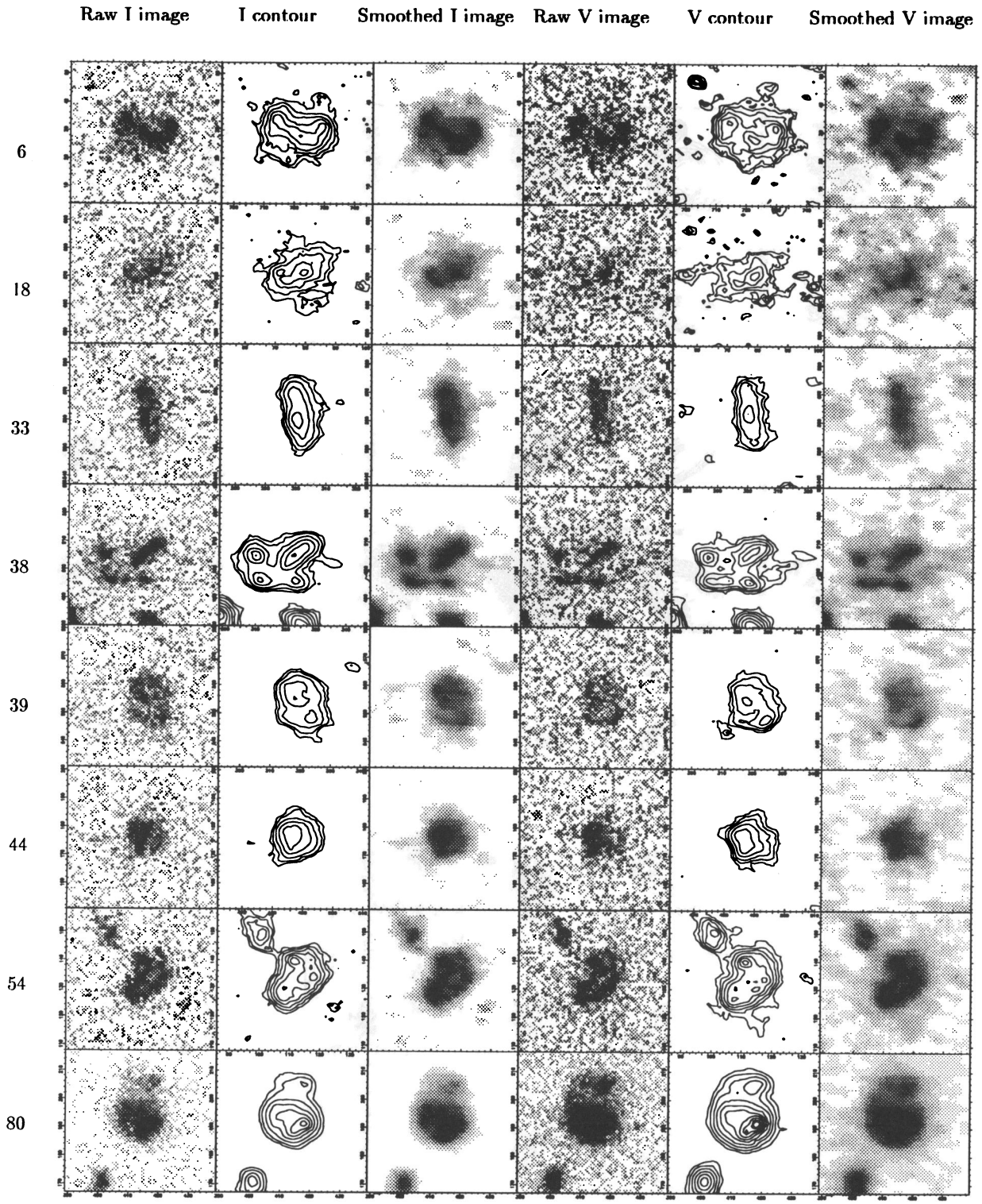

FIG. 10.—For each of the 16 irregular and seven peculiar galaxies, a section of six panels are shown. Each panel represents a 5″ × 5″ box. The panel columns represent the *I*-band image, a contour plot of the *I*-band image smoothed with a 0″.2 FWHM Gaussian, the smoothed *I*-band image, and the corresponding plots in the *V* band. For the first and third columns the data are displayed from $I\mu = 22.0$ to $I\mu = 25.0$ mag arcsec^{-2}. In the seond column, each contour represents an increase in 0.5 mag arcsec^{-2} in SB starting at $I\mu = 24.5$ mag arcsec^{-2}. The fourth and sixth columns are displayed from $V\mu = 23.0$ mag arcsec^{-2} to sky, and the contours for the fifth column are again 0.5 mag arcsec^{-2} intervals in SB, but starting at $V\mu = 25.5$ mag arcsec^{-2}.

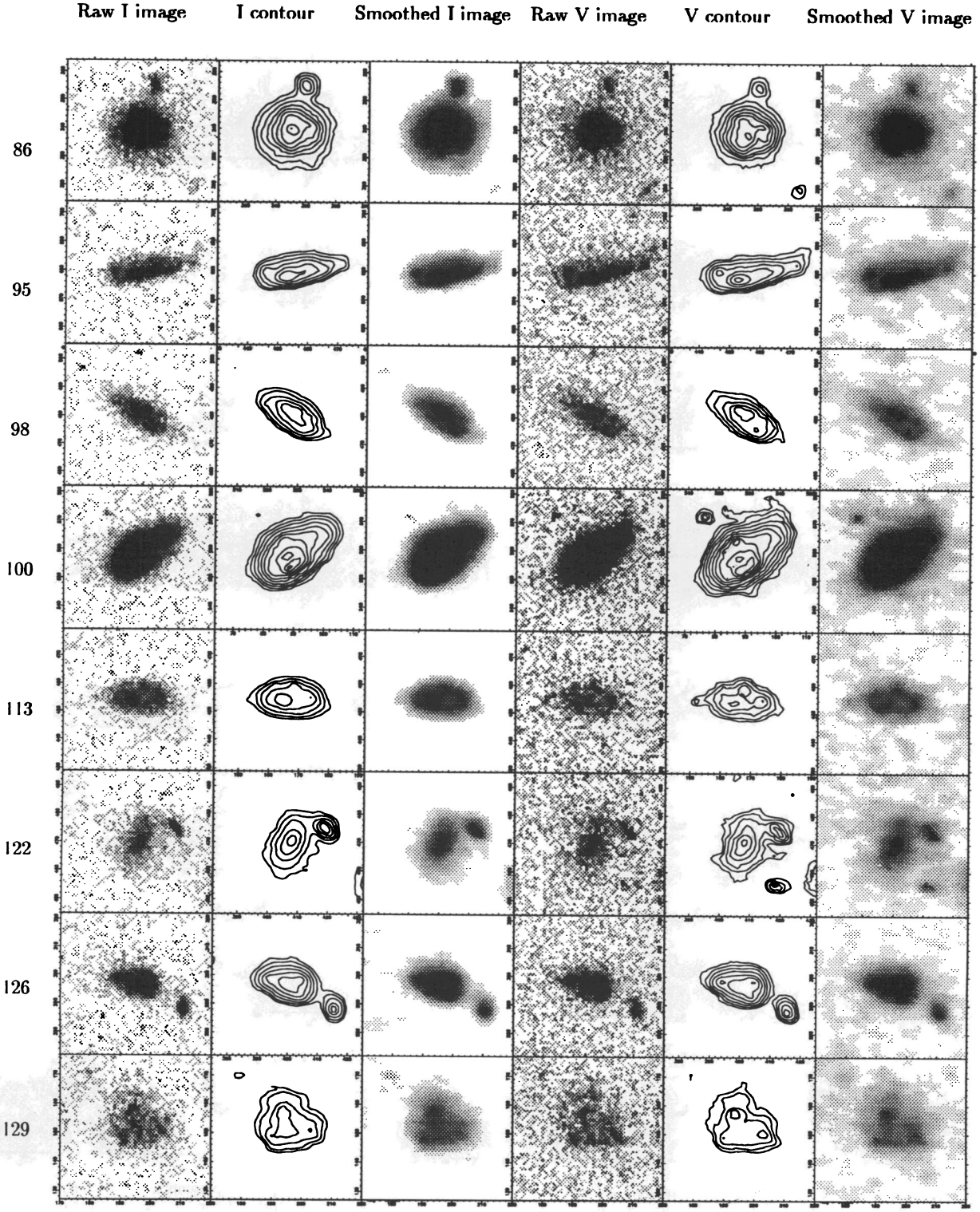

FIG. 10—*Continued*

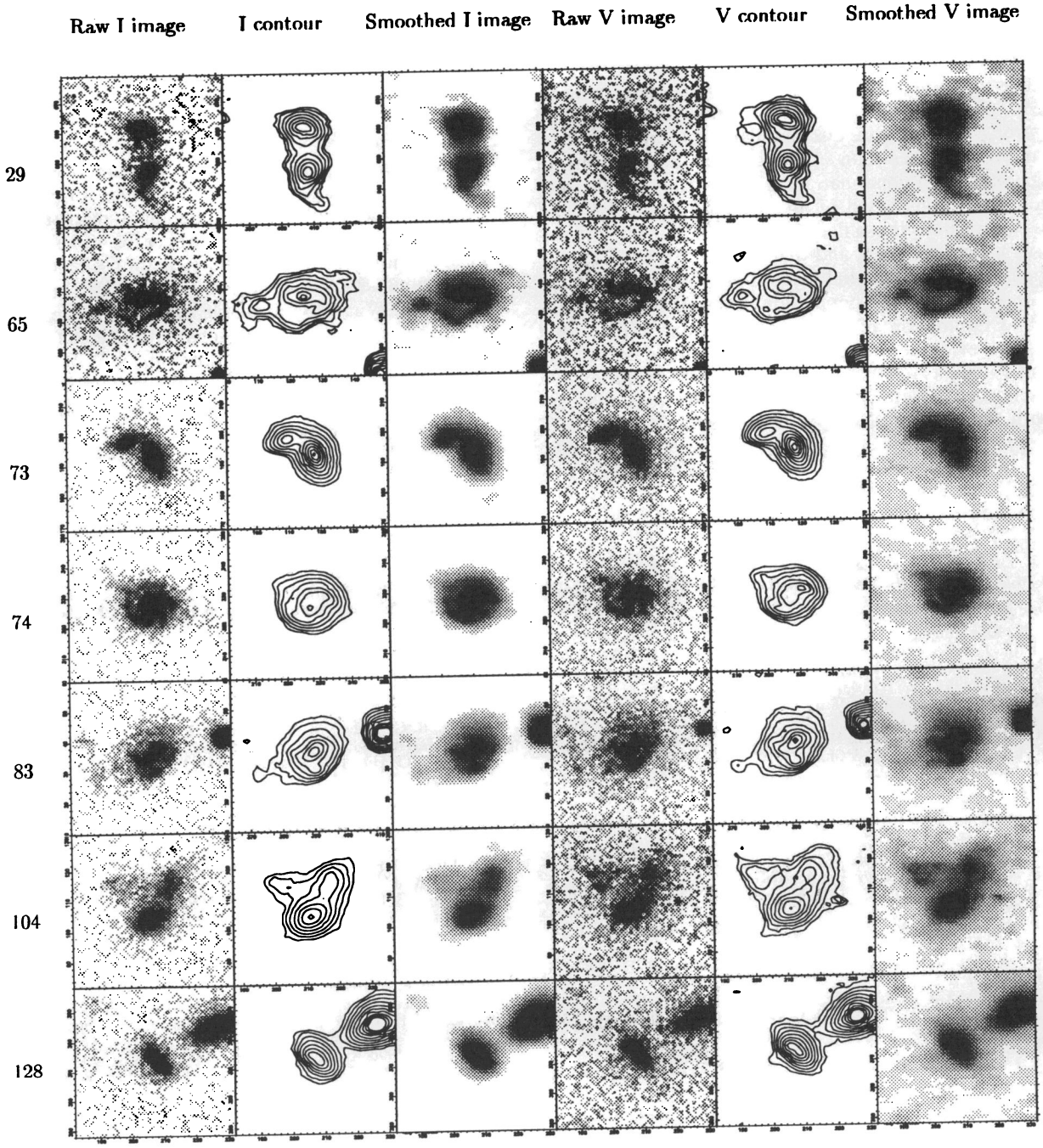

FIG. 10—*Continued*

range $20.0 \leq m_I < 22.0$ mag, with the goal of implementing a full spectroscopic follow-up for all galaxies listed. We have begun such a long-term program at the Multiple Mirror Telescope (MMT) (Driver et al. 1995b). After classification of these galaxies by eye—using both the WFPC2 $V+I$ morphology and light profiles—we compare the global properties of irregulars and late-type spirals to those of ellipticals and early-type spirals. We find little color difference between early- and late-type spirals with mean $(V-I)$ colors of 1.1 ± 0.2 mag. The ellipticals have marginally redder colors with a mean $(V-I) = 1.4 \pm 0.2$ mag. An unexpected number of blue E/S0 systems are identified with $(V-I) < 1.0$ mag. These could possibly be compact narrow emission-line galaxies (cf. Koo et al. 1995). No irregulars are seen with colors redder than $(V-I) = 1.5$ mag. Following the classification method of Forbes et al. (1994), we find that the galaxy types can be reasonably well separated by plotting their concentration index (C.I. = core SB minus total magnitude) versus total magnitude.

We present the differential I-band galaxy number counts as a function of morphological type, excluding those galaxies defined as "peculiar," and conclude that the slopes for the ellipticals and early-type spirals fall at best marginally above the expected prediction from no-evolution models based on conventional Schechter functions and a standard cosmology. Therefore, this implies that strong evolution in the luminous galaxy population is relatively uncommon down to $m_I = 22.0$

mag (i.e., $z \sim 0.5$), as also inferred from the faint galaxy redshift surveys and studies of Lyα absorbers at $z \lesssim 1$ (Steidel, Dickinson, & Persson 1995).

The late-type/irregular galaxies, however, follow a near-Euclidean slope of $[d \log (N)/dm] = 0.64 \pm 0.1$, indicating either strong evolution in this population, local inhomogeneity, and/or a higher than expected *local* space density of dwarf galaxies, or a combination thereof. From detailed no-evolution predictions based on the local LFs of LPEM and MGHC, we conclude that a flat LPEM LF ($\alpha \simeq -1.0$) is *inconsistent* with our *HST* data, and that a steep MGHC LF ($\alpha \gtrsim 1.5$) coupled with a substantial amount of evolution ($\Delta m \sim 1.8$ mag in only $\sim 15\%$ of the population) is more consistent with the data. Examination of the irregulars alone reveals that $\sim 40\%$ show evidence of interactions or multiple core structure, which suggests relatively strong and recent evolution in a large fraction of the late-type population. This work will continue with the study of a deeper field from a 24 orbit *HST* exposure (Driver et al. 1995a), and in a systematic spectroscopic follow-up of the entire current sample (Driver et al. 1995b).

We would like to acknowledge the work of other members of the Johns Hopkins University Medium Deep Survey team (Kavan Ratnatunga, Lyman Neuschaefer, Eric Wyckoff, and Stefano Casertano) in the initial data reduction stage. We would also like to thank Roger Rouse for his help in the galaxy classification process, Dave Burstein for useful and informative discussions, Karl Glazebrook for making his independent MDS galaxy catalog available, Myungshin Im for help with the K-corrections, and the anonymous referee for constructive comments on the original manuscript. S. P. D., R. A. W., and R. E. G. acknowledge financial support from *HST* MDS grant GO.2684.03.93A (Arizona State University) and .01.93A (Johns Hopkins University).

REFERENCES

Babul, A., & Rees, M. J. 1992, MNRAS, 255, 346
Bahcall, J. N., Flynn, C., Gould, A., & Kirhakos, S. 1994, ApJ, 435, L51
Binggeli, B., Sandage, A., & Tammann, G. A. 1988, ARA&A, 26, 509
Broadhurst, T. J., Ellis, R. S., & Glazebrook, K. 1992, Nature, 355, 827
Broadhurst, T. J., Ellis, R. S., & Shanks, T. 1988, MNRAS, 235, 827 (BES)
Burkey, J. M., Keel, W. C., Windhorst, R. A., & Franklin, B. E. 1994, ApJ, 429, L13
Burstein, D., & Heiles, C. 1982, ApJ, 87, 1165
Casertano, S., Ratnatunga, K. U., Griffiths, R. E., Im, M., Neuschaefer, L. W., Ostrander, E. J., & Windhorst, R. A. 1995, ApJ, 453, in press (CRGINOW)
Cawson, M. G. M. 1983, Ph.D. thesis, Univ. Cambridge
Charlot, S., & Bruzual, G. 1991, ApJ, 367, 126
Colless, M., Ellis, R. S., Broadhurst, T. J., Taylor, K., & Peterson, B. A. 1993, MNRAS, 261, 19
Colless, M., Ellis, R. S., Taylor, K., & Hook, R. N. 1990, MNRAS, 244, 408
Colless, M., Ellis, R. S., Taylor, K., & Shaw, G. 1991, MNRAS, 253, 686
Colless, M., Schade, D., Broadhurst, T. J., & Ellis, R. S. 1994, MNRAS, 267, 1108
Condon, J. J. 1989, ApJ, 338, 13
Cowie, L. L., Songalia, A., & Hu, E. M. 1991, Nature, 354, 460
Disney, M. J. 1976, Nature, 263, 573
Driver, S. P. 1994, Ph.D. thesis, Univ. Wales
Driver, S. P., & Phillipps, S. 1995, ApJ, submitted
Driver, S. P., Phillipps, S., Davies, J. I., Morgan, I., & Disney, M. J. 1994, MNRAS, 266, 155
Driver, S. P., Windhorst, R. A., Ostrander, E. J., Keel, W. C., Griffiths, R. E., & Ratnatunga, K. U. 1995a, ApJ, 449, L23
Driver, S. P., Windhorst, R. A., Pascarelle, S. M., & Griffiths, R. E. 1995b, in preparation
Ferguson, H. C., & McGaugh, S. S. 1995, ApJ, 440, 470
Forbes, D. A., Elson, R. A. W., Illingworth, G. D., & Koo, D. C. 1994, ApJ, 437, L17
Giraud, E. 1992, A&A, 257, 501
Glazebrook, K., Ellis, R. E., Santiago, B., & Griffiths, R. E. 1995a, MNRAS, in press (GL95a)
Glazebrook, K., et al. 1995b, MNRAS, 273, 157
Glazebrook, K., Peacock, J. A., Miller, L., & Collins, C. A. 1995c, MNRAS, submitted
Griffiths, R. E., et al. 1994a, ApJ, 435, L49 (GR94a)
———. 1994b, ApJ, 437, 67 (GR94b)
Guiderdoni, B., & Rocca-Volmerange, B. 1987, A&A, 186, 1
———. 1988, A&AS, 74, 185
Hodge, P. 1989, ARA&A, 27, 139
Holtzman, J. A., et al. 1995, PASP, 107, 156
Im, M., Casertano, S., Griffiths, R. E., Ratnatunga, K. U., & Tyson, J. A. 1995a, ApJ, 441, 494
Im, M., et al. 1995b, ApJ, in press
Jones, J. B., Driver, S. P., Phillipps, S., Davies, J. I., Morgan, I., & Disney, M. J. 1995, in preparation
Keel, W. C., & Windhorst, R. A. 1993, AJ, 106, 455
Kent, S. M. 1985, ApJS, 59, 115
Koo, D. C., Gronwall, C., & Bruzual, A. G. 1993, ApJ, 415, L21
Koo, D. C., Guzman, R., Faber, S. M., Illingworth, G. D., & Bershady, M. A. 1995, ApJ, 440, L49
Koo, D. C., & Kron, R. G. 1992, ARA&A, 30, 613 (KK92)
Kron, R. G. 1980, ApJS, 43, 305
Lacey, C. G. 1991, Nature, 354, 458
Lacey, C. G., Guiderdoni, B., Rocca-Volmerange, B., & Silk, J. 1993, ApJ, 402, 15
Lilly, S. J., Cowie, L. L., & Gardner, J. P. 1991, ApJ, 369, 79
Loveday, J., Peterson, B. A., Efstathiou, G., & Maddox, S. J. 1992, ApJ, 390, 338 (LPEM)
Maddox, S. J., Sutherland, W. J., Efstathiou, G., & Loveday, J. 1990, MNRAS, 243, 692
Marzke, R. O., Geller, M. J., Huchra, J. P., & Corwin, H. G. 1994b, AJ, 108, 437 (MGHC)
Marzke, R. O., Huchra, J. P., & Geller, M. J. 1994a, ApJ, 428, 43
McGaugh, S. S. 1994, Nature, 367, 538
Mutz, S. B., et al. 1994, ApJ, 434, L55
Neuschaefer, L. W., Griffiths, R. E., Ratnatunga, K. U., & Valdes, F. 1995, PASP, in press
Neuschaefer, L. W., & Windhorst, R. A. 1995, ApJS, 96, 371
Osterbrock, D. E. 1989, Astrophysics of Gaseous Nebulae and Active Galactic Nuclei (Mill Valley: University Science Books)
Phillipps, S., & Driver, S. P. 1995, MNRAS, 274, 832
Ratnatunga, K. U., Griffiths, R. E., & Casertano, S. 1994, in The Restoration of HST Images and Spectra, ed. R. J. Hanish & R. White, (Baltimore: STScI), 333
Ratnatunga, K. U., Griffiths, R. E., Casertano, S., Neuschaefer, L. W., & Wyckoff, E. W. 1995a, ApJ, submitted
Rocca-Volmerange, B., & Guiderdoni, B. 1990, MNRAS, 247, 166
Sandage, A. 1961, The Hubble Atlas of Galaxies (Washington, DC: Carnegie Institution of Washington Publ. No. 618)
Schechter, P. 1976, ApJ, 203, 297
Shanks, T. 1989, in The Extra-galactic Background Light, ed. S. C. Bowyer & C. Leinert (Dordrecht: Kluwer), 269
Shanks, T., Stevenson, P. R. F., Fong, R., & MacGillivray, H. T. 1984, MNRAS, 206, 767
Steidel, C. C., Dickinson, M., & Persson, S. E. 1994, ApJ, 437, L75
Tyson, J. A. 1988, AJ, 96, 1
Windhorst, R. A. 1984, Ph.D. thesis, Univ. Leiden
Windhorst, R. A., Fomalont, E. B., Partridge, R. B., & Lowenthal, J. D. 1993, ApJ, 405, 498
Windhorst, R. A., Franklin, B. E., & Neuschaefer, L. W. 1994c, PASP, 106, 798
Windhorst, R. A., Gordon, J. M., Pascarelle, S. M., Schmidtke, P. C., Keel, W. C., Burkey, J. M., & Dunop, J. S. 1994b, ApJ, 435, 577
Windhorst, R. A., Mathis, D. F., & Neuschaefer, L. W. 1990, in ASP Conf. Ser., Vol. 10, Evolution of the Universe of Galaxies (Edwin Hubble Centennial Symposium), ed. R. G. Kron (Provo, UT: BookCrafters, Inc.), 389–403
Windhorst, R. A., et al. 1994a, AJ, 107, 930
Wyse, R. F. 1985, ApJ, 299, 593